AD-A193 222 EFFECT OF MICROSTRUCTURE ON THE FATIGUE CRACK PROPAGATION BEHAVIOR OF NI-..(U) GEORGIA INST OF TECH ATLANTA SCHOOL OF MATERIALS ENGINEERING.. 1/2

UNCLASSIFIED S D ANTOLOVICH DEC 87 AFOSR-TR-88-0295 F/G 11/6.1 NL

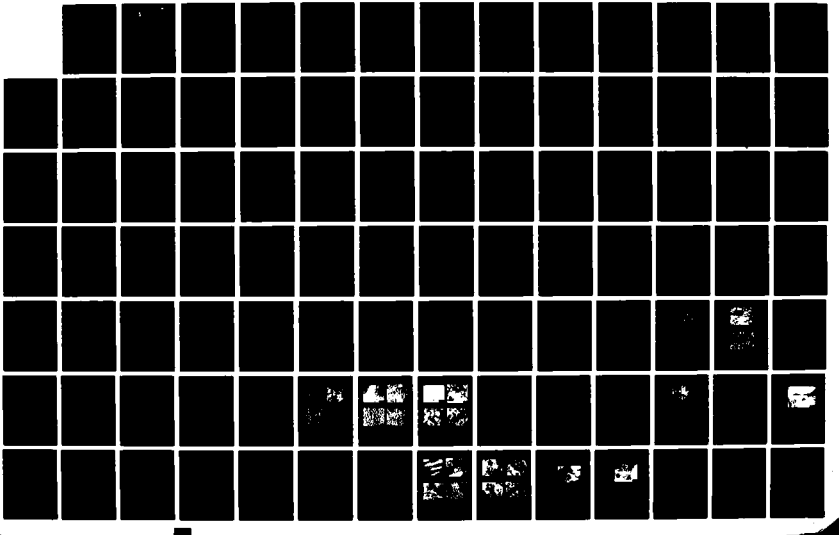

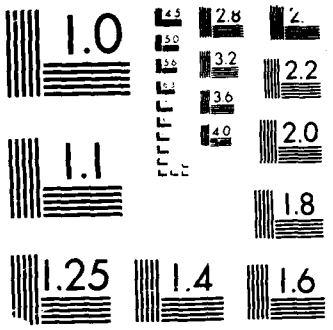

UNCLASSIFIED
SECURITY CLASSIFICATION OF THIS PAGE

(2)

REPORT DOCUMENTATION PA

UTIC FILE COPY

AD-A193 222

DTIC ELECTE MAR 29 1988 S D

1a. REPORT SECURITY CLASSIFICATION: UNCLASSIFIED	1b. RESTRICTIVE MARKINGS
2a. SECURITY CLASSIFICATION AUTHORITY	3. DISTRIBUTION / AVAILABILITY OF REPORT: Approved for public release: distribution is unlimited
2b. DECLASSIFICATION / DOWNGRADING SCHEDULE	
4. PERFORMING ORGANIZATION REPORT NUMBER(S)	5. MONITORING ORGANIZATION REPORT NUMBER(S): AFOSR-TR- 88-0255
6a. NAME OF PERFORMING ORGANIZATION: Georgia Institute of Technology	6b. OFFICE SYMBOL (If applicable)
6c. ADDRESS (City, State, and ZIP Code): School of Materials Engineering Atlanta, Georgia 30332	7a. NAME OF MONITORING ORGANIZATION: Air Force Office of Scientific Research
	7b. ADDRESS (City, State, and ZIP Code): Electronic and Materials Sciences Building 410 Bolling AFB, D.C. 20332
8a. NAME OF FUNDING / SPONSORING ORGANIZATION: AFOSR	8b. OFFICE SYMBOL (If applicable): NE
8c. ADDRESS (City, State, and ZIP Code): Electronic and Materials Sciences Building 410 Bolling AFB, D.C. 20332	9. PROCUREMENT INSTRUMENT IDENTIFICATION NUMBER: AFOSR-84-0101
	10. SOURCE OF FUNDING NUMBERS: PROGRAM ELEMENT NO 61102F; PROJECT NO. 2306; TASK NO A1; WORK UNIT ACCESSION NO.

11. TITLE (Include Security Classification)
Effect of Microstructure on the Fatigue Crack Propagation Behavior of Ni-Base Superalloys

12. PERSONAL AUTHOR(S)
Stephen D. Antolovich

13a. TYPE OF REPORT	13b. TIME COVERED	14. DATE OF REPORT (Year, Month, Day)	15. PAGE COUNT
Technical Report	FROM 5-1-84 TO 9-30-87	December 1987	90

16. SUPPLEMENTARY NOTATION

17 COSATI CODES			18. SUBJECT TERMS (Continue on reverse if necessary and identify by block number)
FIELD	GROUP	SUB-GROUP	Fatigue Crack Propagation, Closure, Ni-Base Superalloys, Mismatch, Microstructure, Anti-Phase Boundary,

19. ABSTRACT (Continue on reverse if necessary and identify by block number)
Aluminum, Titanium, Chromium, Molybdenum

The objective of this study is to determine the effect of microstructural properties on the fatigue crack propagation (FCP) response of Ni-base superalloys. This report describes the results of four experimental alloys containing various amounts of Al, Ti, Cr, and Mo. Chemistry, precipitate size, and grain size were varied to produce systematically controlled microstructures.

The four alloys were characterized for chemical composition, microstructure, tensile properties, low cycle fatigue (LCF), and FCP resistance. The FCP tests were performed under constant load (increasing K) conditions in air at a stress ratio (R) of 0.1 and 0.8. Closure loads were measured with a clip gage, back-face strain gage, and a laser extensometer.

20. DISTRIBUTION / AVAILABILITY OF ABSTRACT: ☒ UNCLASSIFIED/UNLIMITED ☐ SAME AS RPT ☐ DTIC USERS	21. ABSTRACT SECURITY CLASSIFICATION: UNCLASSIFIED
22a. NAME OF RESPONSIBLE INDIVIDUAL: ~~Stephen D. Antolovich~~ Rosenstein	22b. TELEPHONE (Include Area Code): ~~404-894-3012~~ (202) 767-4933
	22c. OFFICE SYMBOL: NE

DD FORM 1473, 84 MAR 83 APR edition may be used until exhausted. All other editions are obsolete.

SECURITY CLASSIFICATION OF THIS PAGE
UNCLASSIFIED

ABSTRACT

The objective of this study is to determine the effect of microstructural properties on the fatigue crack propagation (FCP) response of Ni-base superalloys. This report describes the results of four experimental alloys containing various amounts of Al, Ti, Cr, and Mo. Chemistry, precipitate size, and grain size were varied to produce systematically controlled microstructures.

The four alloys were characterized for chemical composition, microstructure, tensile properties, low cycle fatigue (LCF), and FCP resistance. The FCP tests were performed under constant load (increasing K) conditions in air at a stress ratio (R) of 0.1 and 0.8. Closure loads were measured with a clip gage, back-face strain gage, and a laser extensometer.

Through compositional control the lattice mismatch, anti-phase boundary energy (APBE), and volume fraction of gamma prime precipitates were systematically varied. Heat treatments were utilized to obtain two gamma prime sizes.

Constant amplitude cycling revealed distinct differences in FCP response between the four alloys. To determine the role of crack tip shielding in controlling FCP rates closure loads were measured. The back-face strain gage and clip gage proved to be unreliable in measuring closure by noting the change in slope of a load-displacement curve. Non-linearity in the output was associated with factors other than crack closure. The laser extensometer, however, provided reproducible results based on the

consistently linear output obtained from an uncracked calibration specimen.

Based on the FCP response of these alloys it was determined that crack closure concepts did not explain the differences in FCP rates in the model Ni-base alloys studied. FCP rates were dramatically reduced for those compositions and heat treatments that promoted planar, reversible slip. The alloys having high volume fraction, low APBE, and low mismatch exhibited FCP rates that were approximately 50 times lower than other treatments.

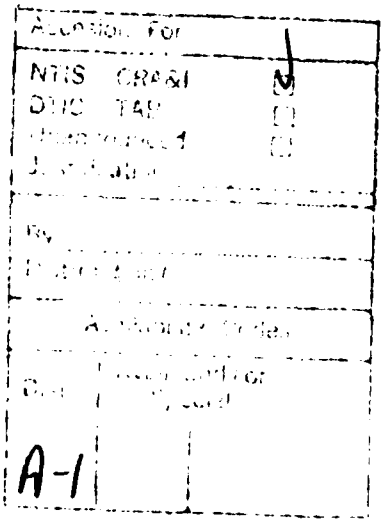

CONTENTS

CONTENTS

ILLUSTRATIONS

ILLUSTRATIONS

ILLUSTRATIONS

TABLES

ABBREVIATIONS AND SYMBOLS

a	Crack Length
APB	Anti-Phase Boundary
APBE	Anti-Phase Boundary Energy
CRSS	Critical Resolved Shear Stress
COD	Crack Opening Displacement
CTOD	Crack Tip Opening Displacement
da/dN	Crack Growth Rate
E	Elastic Modulus
FCC	Face Centered Cubic
FCP	Fatigue Crack Propagation
K	Stress Intensity
K_{cl}	Stress Intensity at Closure
K_{eff}	Effective Stress Intensity Factor
K_{Ic}	Plane Strain Fracture Toughness
K_{th}	Threshold Stress Intensity
LCF	Low Cycle Fatigue
R	Stress Intensity Ratio (P_{min}/P_{max})
R_f	Linear Roughness Parameter
SEM	Scanning Electron Microscope
TEM	Transmission Electron Microscope
V_f	Volume Fraction
γ	Alloy Face Centered Cubic matrix
γ'	Ordered Precipitate
δ	Lattice Mismatch
Γ	Anti-Phase Boundary Energy

1. INTRODUCTION

Jet engine components are fabricated almost entirely from Ni base superalloys. These alloys contain elements that are in short supply in the United States. Consequently, they must be imported, in many cases from countries that are politically unstable. The lack of domestic resources makes our supply subject to interruption through unavailability. There is thus a major emphasis to save "strategic" materials and programs have been undertaken in which Ni was substituted for certain strategic materials, usually Co,Ta,Cr, and Nb.

The problem with that approach is two-fold. Firstly, there is ample evidence that the classification of what is strategic is continually changing. Thus a non-strategic material can become strategic and visa-versa depending on the economic conditions. Secondly, a simple substitution is almost certainly not the approach that will conserve the most materials. If a component can be made by reducing the level of a given element by 25% and if the life of the component is reduced 50%, then there is a net increase in the use of that element and all other elements in the component of interest when computed over the life of the engine or aircraft.

The most logical approach, and the one that has not been fully exploited, is to develop an understanding of the interactions amongst the alloying elements and to use that understanding to develop alloys which last much longer in

service. Thus even if there is an increase of 25% in a given element or elements, if this produces a doubling of the life, a large reduction in the use of the materials will be accomplished.

Fatigue crack propagation (FCP) has been chosen as the target property since with the introduction of Retirement-for-Cause philosophy (RFC) [1] it has become, for the first time, design-critical for turbine disks. Furthermore, disks constitute up to 70% of the total engine weight, therefore any material savings are greatly magnified.

The goals of this research were therefore;

1) Develop a set of alloys in which fundamental microstructural properties are manipulated through compositional control and heat-treatments.

2) Develop models based on mechanical test results and fundamental observations which will identify key variables and predict FCP rates.

3) Use this information to suggest alterations in existing alloy systems to improve FCP resistance which thereby producing material savings over the life of the component.

These goals were addressed by evaluating a series of alloys subjected to low cycle fatigue (LCF) along with tensile and FCP tests. Specimens were analyzed using transmission electron microscopy (TEM), scanning electron microscopy (SEM), optical microscopy, and x-ray diffraction in an effort to identify those mechanisms responsible for damage accumulation and thus crack growth in Ni base alloys.

2. BACKGROUND

2.1 Metallurgy of Ni-Base Superalloys

The complexity of the composition of Ni-base alloys can be overwhelming. In the majority of commercial alloy systems as many as 12 or 13 alloying elements can be present in addition to as many trace elements [2]. In most systems however, the major components include Ti, Al, Cr, Mo, in addition to the Ni. The effect of each of these constituents on the microstructure is relatively well known. What is less well understood is how the microstructural features affect mechanical properties. This point will be discussed in more detail later.

Superalloys consist of a face centered cubic (FCC) solid solution, γ, an ordered FCC precipitate (Figure 1), γ', and various carbides and borides. The γ matrix is a solid solution of Ni with substantial amounts of Cr. Other elements commonly found in the γ phase of modern superalloys include Co, W, Mo, Al, and Ta which serve as solid solution strengtheners. Superalloys contain from 15 to 70 volume percent γ', an ordered phase based on Ni_3Al. Titanium, Nb, and Ta, are common additions which replace Al atoms, in γ', whereas Co substitutes solely for Ni.

The γ' phase is useful for a number of reasons. The precipitate is coherent with the matrix, due to the small difference in the lattice parameter of the matrix and the precipitate (typically on the order of 0.01 - 0.5%). This small

mismatch allows for homogeneous nucleation of the γ' and stability at elevated temperatures. Figure 2 shows the γ' morphology for two alloys with different lattice mismatch. Gamma prime, unlike most materials, shows an increase in strength with increasing temperature [3]. Anti-phase boundary (APB) strengthening due to the γ' phase is also a major strengthening contribution of γ'.

2.2 Mechanical Properties of Ni-Base Superalloys

The yield strength of nickel-base superalloys is relatively high at room temperature, and remains high up to about 750° C. This strength is primarily due to the presence of the γ' phase which has the unique property of increasing flow stress with increasing temperature (Figure 3). The strength is a function of both the properties of the phases and how the γ' is dispersed in the alloy. Some important factors include solid solution strengthening of γ and γ' , anti-phase boundary energy (APBE) of the γ', coherency strains between the γ and γ', and volume fraction, particle shape, and particle size of γ' [2]. Solid solution hardening of γ involves the increase in flow stress resulting from changes in lattice parameter, elastic modulus, stacking fault energy, and other mechanisms.

Many investigators have studied the increase in yield stress of γ' as a function of temperature [3-11]. This phenomena is considered to be the result of thermally assisted cross slip of 1/2<110> dislocation from {111} planes to {100} planes. It is

suggested that only the leading dislocation cross slips onto the cube plane, making the pair immobile and thus creating an obstacle to further deformation. The decrease in yield stress above 750° C is caused by the onset of primary cube slip, in which both dislocations move on the {100} planes [12].

Several mechanisms by which γ' precipitates act to impede dislocation motion have been proposed. For small particle sizes, the γ' particles are usually sheared by a pair of dislocations. Shearing by the leading dislocation creates an APB resulting in an increase in energy. Passage of a second dislocation through the γ' restores the stacking sequence thereby eliminating the APB. The stress necessary to shear the precipitate was calculated by Ham [13] to be;

$$\tau_c = \frac{\Gamma^{3/2}}{b} \left(\frac{4 f r_s}{\pi T} \right)^{1/2} \quad . \quad . \quad . \quad (1)$$

where

Γ = APBE
f = volume fraction
b = Burger's vector
r_s = average dimension of particle intersected by a slip band. $(2/3)^{1/2}\ r_0$
r_0 = particle radius
T = dislocation line tension

Larger γ' particles are, on the other hand, by-passed by the Orowan looping mechanism. In this process the CRSS of an edge dislocation is [14];

$$\Delta\tau = \frac{Gb}{2\pi L}\ \phi'\ \mathrm{Ln}\left(\frac{L}{2b}\right) \quad . \quad . \quad . \quad (2)$$

where

G = shear modulus
b = Burger's vector
$\phi' = 1/2(1+1/(1-\upsilon))$
L = square lattice spacing
$= (2\pi/3f)^{1/2} r_0$
r_0 = particle size

In order for shearing to occur the stress necessary for particle cutting must be less than the Orowan looping stress (Figure 4). Both the cutting and shearing stresses are a function of the γ' properties and particle size thus allowing the deformation process to be controlled through manipulation of microstructure and chemistry.

2.3 Microstructural Features

2.3.1 Mismatch

The gamma prime precipitate remains ordered up to temperatures as high as 1000° C [15]. Due to the difference in lattice parameter between the matrix and precipitate, a strain field exists around the γ' which influences the motion of dislocations. Mismatch is defined by;

$$\delta = 2\left(\frac{a_{\gamma'} - a_{\gamma}}{a_{\gamma'} + a_{\gamma}}\right) \quad . \quad . \quad . \quad (3)$$

where

a_{γ} = lattice parameter of the matrix
$a_{\gamma'}$ = lattice parameter if the precipitate

The influence of γ' mismatch on the critical resolved shear stress (CRSS) of an alloy is related to the interaction between

the dislocations and the associated strain field. The increase in flow stress due to the strain field/ dislocation interaction is described by the following equation [16];

$$\Delta\tau = 3G\delta^{3/2}\left(\frac{r_o}{b}\right)^{1/2} \quad . \quad . \quad . \quad (4)$$

where

$\Delta\tau$ = increase in flow stress
G = shear modulus
δ = mismatch
r_o = particle radius
b = Burger's vector

This equation predicts that the flow stress should increase somewhat more rapidly than δ, because increased misfit bends the dislocation more resulting in greater interaction with the strain field.

2.3.2 Anti-Phase Boundary Energy

Below a critical γ' size, dislocations no longer bow between the particles; instead, the dislocations move by particle shearing. Copley and Kear [17] modified the Gleiter-Hornbogen theory of particle shearing to predict CRSS. The rate controlling step for plastic deformation was shown to be moving the leading dislocation from the γ to the γ'. Motion of a unit dislocation through the γ' creates an APB. Passage of a second dislocation restores order and eliminates the APB. For conditions of static equilibrium the following equation was derived;

$$\tau_c = \frac{\Gamma}{2b} - \frac{T}{br_0} + 1/2 \quad (\tau_0 + \tau_p) \quad . \quad . \quad . \quad (5)$$

where

Γ = APBE
r_0 = particle radius
k = constant
τ_p = friction stress of the particle
τ_0 = friction stress of the matrix

A major contribution to τ_c at room temperature is provided by the term $\Gamma/2b$. Leverant et. al [18] concluded, however, that at high temperatures and high strain rates both the APBE and flow stress of the γ' are major contributors to τ_c.

2.3.3 Grain Size

Many investigators have shown grain size to have an effect on FCP rates [19-24]. In general, it appears that increasing the grain size reduces the FCP resistance of the material, however, the mechanism for this behavior is still debated.

Antolovich et. al [25] proposed that a LCF process occurs at the crack tip region some distance 'ρ' ahead of the main crack. In this model, FCP is caused by damage accumulation in small elements ahead of the crack tip that are subjected to reverse yielding. The crack then advances by some distance when sufficient damage has accumulated in this "process zone". It was found that longer FCP lives are associated with larger process zones. The larger the process zone the smaller the average strain and the greater the number of cycles required to accumulate a

critical amount of damage and advance the crack. Larger grain sizes increase the inhomogeneity of deformation and thus the amount of slip reversibility. Inhomogeneous deformation, in which dislocation motion is restricted to well defined slip planes giving rise to less dislocation interaction. Therefore in planar slip materials there is less resistance to further dislocation motion resulting in less damage accumulation and longer FCP lives.

Alternatively, other studies [26-28] attribute the reduction in FCP rates of coarse grain materials to increased amounts of crack closure. The concept of closure is discussed in detail in the next section. Closure results in a reduction of the stress intensity at the crack tip due to crack tip shielding of the remotely applied load. They found that the improvements in FCP resistance with the larger grains did not exist at high R -ratios where closure does not occur. The coarse and fine grained materials had nearly the same growth rates for R = 0.8. The explanation is that the larger grain sizes increases the fracture surface roughness resulting in more roughness induced closure. Also, the larger grains and correspondingly rougher surfaces resulted in a greater effective crack path. Both of these effects contribute to a reduction in the FCP rates.

2.4 Closure

Elber [29] discovered a complicating factor in the correlation of crack growth rates with applied ΔK due to the

phenomena of crack closure. Closure is thought to shield the crack tip such that the effective stress intensity ($K_{eff} = K_{max} - K_{cl}$) is less than that which is calculated using the remotely applied loads. In Elber's model, closure is due to crack growth through the plastic zone wake, resulting in crack face contact before zero load. This effect has since been called plasticity induced closure [30].

Another closure mechanism exists when the fracture surface is irregular and local mode II displacements are present. In this case, premature crack face contact occurs preventing the crack from closing completely thereby reducing the magnitude of cyclic loading at the crack tip. This mechanism is termed roughness induced closure [31]. Roughness induced closure is expected to operate only when the size of the surface asperities is comparable to the crack tip opening displacement(CTOD). This condition is present in near threshold tests or at low R-ratios.

Regardless of the mechanism, closure results in a decrease in the driving force for crack growth. Cyclic loading between an upper limit P_{max} and a minimum P_{min} produces a cyclic stress intensity range described by ΔK. It is the magnitude of ΔK, as well as the R-ratio, which governs the rate of crack growth. If the crack is held closed or wedged open the effective cyclic load transmitted to the crack tip is reduced resulting in a lower driving force for crack advance.

2.5 Fatigue Crack Propagation Models

As mentioned earlier, predicting the growth rate of preexisting flaws is a primary concern in today's engineering structures. The Air Force's Retirement-for-Cause philosophy requires that given a crack size and loading conditions, the useful remaining life in a component must be calculated. To this end there is no shortage of models in existence which predict crack growth rates under various stress conditions. Perhaps the most familiar model is the Paris model which states [32];

$$\frac{da}{dN} = C(\Delta K)^m \qquad . \quad . \quad . \quad (6)$$

where C and m are constants and ΔK is the stress intensity parameter range. This is an empirical model which fits the results of da/dN vs. ΔK on a log- log plot. This equation is restricted to a limited range of ΔK, bounded at high ΔK by K_{Ic}, the fracture toughness, and at low ΔK by ΔK_{th}, the level below which long cracks appear not to grow. Many other attempts have been made since the work of Paris to include other effects into this model such as R-ratio (min stress/max stress), Young's modulus, yield stress, etc.). An example of this is the equation by Forman [33];

$$\frac{da}{dN} = \frac{C\Delta K^n}{(1-R)K_c - \Delta K} \qquad . \quad . \quad . \quad (7)$$

Although these models fit the data well and allow some degree of confidence in predicting FCP lives, they give no clue as to the underlying mechanism for the crack growth process. Development of FCP resistant materials requires a detailed knowledge of the mechanism responsible for crack extension.

A more detailed FCP model was proposed by Antolovich, Saxena, and Chanani [25] in which the LCF process is assumed to occur ahead of the crack tip. The process zone occurs at a distance "ρ" ahead of the crack tip producing a crack advance of "ρ" units in ΔN cycles, where ΔN_i is the number of cycles to crack initiation at an average plastic strain range $\Delta\varepsilon_p$ in the process zone. ΔN_i can be calculated from the Coffin-Manson equation:

$$(\Delta N_i)^{\beta}\Delta\varepsilon_p = C_0\varepsilon_f \quad . \quad . \quad . \quad (8)$$

where

N_i = cycles to initiate crack in process zone
β = Coffin-Manson exponent
ε_p = plastic strain range
ε_f = fatigue ductility
C_0 = constant

From this the following equation results:

$$\frac{da}{dN} = \frac{C}{(\sigma_{ys}\varepsilon_f E)^{1/\beta}} \frac{1}{\rho^{1/\beta-1}} \Delta K^{2/\beta} \quad . \quad . \quad (9)$$

where

σ_{ys} = cyclic yield
E = Young's modulus
C = constant

Finally there are the models which are based on dislocation activity at the crack tip. These models are the most general and fundamental but unfortunately in order to solve the problems the conditions must be very idealized. An example of this approach was proposed by Wertman [34]. In this model it is assumed that the crack will grow to a length, Δa, if a critical value D_c of the accumulated displacement is reached. Mathematically, D_c is given by the equation

$$D_c = \Sigma |D_n| \qquad . \quad . \quad . \quad (10)$$

where D_n is the displacement increment that occurs across the crack plane at a fixed point during the n_{th} cycle. After some assumptions and substitutions it is found that

$$\frac{da}{dN} = \frac{A\Delta K^4}{G\sigma_{ys}U} \qquad . \quad . \quad . \quad (11)$$

where

n = strain hardening exponent
G = shear modulus
σ_{ys} = monotonic yield stress
K = stress intensity parameter
U = energy per unit crack advance

This model indicates than an accumulated displacement criterion leads to a 4th-power Paris equation. Such a criteria is in fact equivalent to an accumulated plastic work criterion. The details of these and other models are presented in a comprehensive review of FCP models by Bailon and Antolovich [35].

There is currently a strong controversy in the research community concerning the relative effects of closure on FCP rates. Proponents of intrinsic microstructurally controlled FCP claim increased resistance to FCP is achieved by obtaining a high degree of slip reversibility resulting from planar slip as previously discussed. Supporters of closure mechanisms claim microstructure has a second order effect in that it controls the amount of closure which occurs. A planar slip material generally forms cracks along slip bands resulting in a fairly rough fracture surface which potentially increases the magnitude of the roughness induced closure. Supporters of closure mechanisms claim that if the da/dn vs. ΔK results were normalized with respect to K_{eff}, microstructural differences would play a small role in controlling FCP rates. To some degree, the results predicted by these two different rationales arrive at the same conclusions concerning microstructure and crack growth rates, i.e. planar slip increases crack growth resistance, only the mechanism is different.

In some cases (e.g. high R -ratio, short cracks, some materials) closure does not occur and it becomes important to establish whether the FCP rates can be modified through an intrinsic effect of the microstructure or if these microstructural changes are useless in a regime where closure does not operate. The goal of this project was to isolate the effect of each variable described in the preceding section

through the use of carefully prepared experimental Ni base superalloys.

Previous work on FCP dealt with commercial alloys in which the microstructural features were not fully and systematically controlled. This makes the task of decoupling the individual microstructural effects very difficult if not impossible. In addition, the vast majority of previous work has not addressed the potential effects of closure in the interpretations. Unfortunately, to-date no ASTM standard exists concerning closure measurements. Incorporating closure in any analysis therefore requires development of an accurate measurement technique. In view of these facts the present work represents one of the most precise analysis of factors influencing FCP in Ni base superalloys thus far.

3. RESEARCH PROGRAM

3.1 Alloy Preparation and Processing

It was stated earlier that the Ni-Ti-Al-Cr-Mo system is promising for reasons previously discussed. Obviously it is not practical to vary all the elements in an effort to obtain the ideal alloy. Instead, results of previous investigations were used where those studies resulted in microstructures that appear promising for reduced FCP rates. These compositions were used as a starting point and variations in chemistry to investigate particular factors were made. Powder metallurgy (PM) approaches were avoided because prior particle boundaries can contain impurities which can mask or reduce microstructural effects. Conventional ingot metallurgy (IM) approaches avoid any such problems. Since production of the ingots is an expensive operation it was important to firmly establish the correct compositions prior to alloy production. The microstructural variables included APBE (Γ), mismatch (δ), volume fraction of γ' (V_f), and superimposed was grain size and γ' size which were controlled by heat-treatments.

3.1.1 Anti-phase Boundary Energy

Anti-phase boundary energy control was achieved through the Ti/Al ratio. It has been shown [36] that the APBE of γ' precipitates is directly related to the Ti/Al ratio of the alloy.

This, therefore, provides a convenient method of determining the composition required to produce the APBE values desired. The object of this set of experiments was to maintain a relatively constant volume fraction and mismatch for the γ' while varying the Ti/Al ratio thereby controlling APBE. In particular, while maintaining a low mismatch, alloys having high and low APBE were prepared (Table I).

3.1.2 Mismatch

This effect was investigated by having alloys with a low APBE and having both high and low mismatch. In this case alloy 1 in Table I. served as the low mismatch material and alloy 3 has high mismatch. Assuming a linear relationship between APBE and Ti/Al ratio, the APBE changes by a factor of 1.3 while the mismatch changed by a factor of 20. It was desirable to slightly increase the Al and Ti while keeping their ratio constant in order to increase the γ' volume fraction while leaving the mismatch and APBE unaffected. Presumably, a high mismatch leads to a higher degree of wavy slip than the low mismatch.

3.1.3 Volume Fraction

Since strength is important in disk alloys, it is desirable to investigate strength variations for alloys which show good fatigue resistance. Such alloys are likely to be those for which slip is most planar and most reversible. This effect can be studied by comparing alloys 1 and 2 which have the same APBE and

mismatch but different Al contents and thus different γ' volume fractions. It would be expected that via this approach both the strength and fatigue resistance could be enhanced.

3.1.4 Heat Treatment

The chemical compositions discussed in preceding sections should have different degrees of planar slip and slip reversibility for a given heat treatment. These effects can be significantly varied by performing different heat treatments. It would be ideal to heat treat each alloy to produce two distinct microstructures. The first being one with large grains and small γ'. The resulting structure promotes deformation by particle shearing and planar slip. The second being small grains and large γ' to ensure homogeneous deformation by looping. These two microstructures provide the extremes in deformation behavior (and presumably FCP performance) and supply information about the relative efficiency of composition control vs. heat treatment in controlling FCP rates.

3.1.5 Initial Heats

Prior to production of the 100 lb. ingots to be used as stock material in this study it was decided to prepare some test heats to determine if the desired microstructural properties would be obtained. NASA Lewis Research Center in Cleveland Ohio was very helpful in this regard by preparing small 50 gm. test heats for subsequent microstructural examination at Georgia Tech.

Using this information modifications in compositions were suggested as needed and further test heats were produced. Several attempts were required before deciding on the final compositions shown in Table I.

3.1.6 Ingot Processing

One of the most significant aspects of this project was the ability to isolate the microstructural parameters. Previous FCP studies have typically used alloy systems in which the microstructural variables of interest were not independently varied. Observed differences in FCP resistance were due to a particular combination of many factors wherein the effects of the individual variables had been masked.

In an effort to keep as many variables constant as possible from specimen to specimen it is hoped that during the processing, grain size and composition would be uniform throughout the ingot. If this were not the case, the FCP response of a certain alloy would depend on position in the ingot from which the specimen was taken. Fortunately, Wyman-Gordon has developed a technique whereby ingots can be hot pressed into pancake shapes with a uniform composition and distribution of grains throughout. The processing involves a repetitive cycle of hot pressing and homogenization at temperatures specific to each alloy's composition. Wyman-Gordon's assistance was extremely valuable to this project since the homogeneous ingots could not have been obtained elsewhere.

3.2 Microstructural Measurements

3.2.1 Volume Fraction

Using TEM micrographs to determine volume fractions involves the complication of a two dimensional representation of a three dimensional foil. In TEM micrographs the images are projected onto a plane. Consequently, overlap and truncation of the particles must be considered. Using stereological equations a determination of volume fraction from a measurement of area fraction is possible. Several assumptions are made in developing these equations such as assuming a random distribution of spherical particles. Underwood [37] derives the following equation for calculating volume fraction from area fraction in a projected image;

$$V_V = A_A \frac{2D}{2D + 3t} \qquad \ldots\ldots (12)$$

where

V_V = volume fraction
A_A = projected area fraction
D = diameter of uniform spheres
t = foil thickness

To increase the confidence in the TEM approach of volume fraction determination, the more direct technique of phase extraction was used as well. In this method the γ' phase was separated from the γ matrix and other phases present. Since the density of γ' is only 5% less than the γ matrix, the difference

between weight fraction (as measured by extraction) and volume fraction (from TEM) is ~1% for a 20 weight percent γ' alloy.

The apparatus used for the extraction consisted of a d-c power source in which the cathode is a 40 cm^2 platinum mesh. The specimen was welded to a platinum wire and serves as the anode. Ammonium sulfate and citric acid are mixed in a 250 ml beaker with distilled water. Applying a current dissolves the matrix and leaves only the γ'. By knowing the specimen weight before and after the extraction a weight percent γ' can be calculated.

3.2.2 Mismatch

Mismatch can be determined using X-ray diffraction. If it is possible to resolve the two peaks corresponding to the γ and γ' it is possible to calculate the lattice parameter using the following equation;

$$a = \frac{\lambda(h + k + l)}{2 \sin \theta} \qquad \ldots\ldots\ldots (13)$$

where

a = lattice parameter
λ = X-ray wavelength
θ = angle corresponding to X-ray intensity peak
h,k,l = Miller indices of reflecting planes

Mismatch is affected by temperature and by the state of internal stress in the specimen. There is some loss of generality therefore when using the room temperature measurements to explain behavior of the high temperature tests. However, extensive

elevated testing is not planned since the FCP critical parts of turbine disks are relatively cool. (High temperature determination of misfit may be performed at a later date when the high temperature x-ray camera becomes available.)

3.2.3 Anti Phase Boundary Energy

The most widely known method of measuring APBE is to measure the equilibrium separation of two total dislocations. Movement of the first dislocation through the γ' creates APBE in its wake while the second restores the order. The distance between this pair is inversely related to the energy of the fault. A simple force balance results in the following equation;

$$\Gamma = \frac{G\, b_1\, b_2}{2\pi dkf} \qquad . \quad . \quad . \quad (14)$$

where

Γ = APBE
G = shear modulus
b = Burger's vector
k = 1 for screw pairs and $(1-\nu)$ for edges
d = separation between pairs
f = fraction of dislocation line intercepted by particles

3.3 Fatigue Crack Propagation

The FCP specimen geometry is shown in Figure 5. Tests were performed primarily at room temperature using a closed loop servo-hydraulic test machine. Testing started in the near-threshold region and covered approximately three orders of magnitude in growth rate. Crack lengths were monitored with a d-c

potential drop system. In addition, crack closure was measured by compliance (load/displacement) techniques. Testing was performed at an R-ratio of 0.1 and 0.8 to examine the effect of closure.

3.3.1 Closure

Extensive research on the effects of microstructure on FCP has been conducted on a variety of metal systems. In particular, the effect of grain size on FCP has received considerable attention. Closure has been investigated recently by many investigators in an attempt to explain crack growth results. Crack closure can include plasticity induced closure, crack tip corrosion products, or roughness induced closure. No conclusive evidence has been offered to prove or disprove this effect to date. The different R-ratio tests were performed to determine whether closure is playing a role in this set of experiments.

The basic idea behind most measurements of closure is to record the load vs. strain or displacement during the loading or unloading portion of the cycle. If the crack is held closed due to plasticity or wedged open as in roughness or oxide induced closure, a change in the compliance should occur as the crack faces separate during loading as in Figure 6. The closure load, P_{op}, is then taken to be the load at which the change in compliance occurred.

The vast majority of closure work has been performed on compact tension(CT) specimens. It has been shown by Richards and Dean [38] that crack length can be correlated to the strain on

the back face of the specimen. Tensile loading on a CT specimen produces a negative strain on the back face which is then used to calculate the crack length. During the loading cycle a change in slope of the back face strain vs. load curve indicates the crack has opened. This is an indirect measure of closure since the displacement of the crack tip is not directly measured.

Another technique utilizes a clip on gage which monitors the load line displacement at the mouth of the specimen. The measurement can also be performed with the clip gage attached to the front face of the specimen. This avoids the extra machining required to accommodate the clip gage at the load line. This is a more direct measure of closure than the back face strain gage (BFSG) however the displacements very near the crack tip can not be measured due to the size of the clip gage.

A much more accurate method has been developed by Davidson and Lankford. It involves direct measurement of crack opening displacement (COD) by means of an in-situ SEM loading stage[39]. It is possible to observe COD very near the crack tip. Unfortunately this technique is not available to most laboratories. Alternatively, any device capable of measuring displacement on the specimen could be used for closure measurements. Therefore it was decided to use a laser extensometer and to compare the results to those obtained from the BFSG and clip gage. The laser extensometer measures the gap between the crack face at any point along the machined notch, Figure 7. Any position along the notch can be used by simply

translating the laser to a new position without interrupting the test. The limitation of the instrument used in this project is that the minimum separation of the two surfaces must be greater that about 0.08" and the frequency of the test must be reduced to 0.1 Hz. Each specimen was polished prior to testing to facilitate observation of slip bands using optical microscopy.

The fracture surface was digitized using a method described elsewhere [40] to determine the roughness parameter R_f (R_f = total crack length/projected length).

3.4 Tensile Tests

Each composition was tested to failure under strain control at a rate of 0.5%/min at room temperature. This provided information on yield stress and Young's modulus which is needed for choosing the appropriate loads in the FCP and LCF tests. In addition, TEM examination of the tested specimens provided information concerning the deformation mode for each composition.

3.5 Low Cycle Fatigue

LCF tests were performed to provide information about the effect of microstructure on cyclic deformation. Only one strain range was used. Each test was conducted in total strain (zero-tension-zero) control such that 0.2% plastic strain was obtained at saturation. These conditions were chosen so as to simulate the conditions at the crack tip as realistically as possible.

4. RESULTS AND DISCUSSION

This section describes the results obtained on the small grained alloys designated as indicated in Table I. For ease of presentation the alloys have been numbered according to their composition and gamma prime size. Therefore alloy number one with small γ' size is referred to ad 1S while the large γ' material is 1L, etc. A summary of the alloys' properties is presented in Table II.

4.1 Initial Microstructures

As mentioned in the experimental procedure section, the alloys were formed into "pancakes" by Wyman-Gordon prior to specimen fabrication. The grain size is very uniform across the entire cross section with an average grain size number of 8. This homogeneity of grain size in the pancake is essential if similitude is desired from one specimen to another of the same composition. Higher magnification optical micrographs of each alloy and γ' size are shown in Figures 8-9. These micrographs show the alloys to be free from any defects such as inclusions , porosity, etc. The γ' is unresolvable in the optical micrographs for the S series of alloys whereas in the L series the γ' is clearly visible. There is some preference for γ' formation along the grain boundaries in the L series but the distribution is relatively homogeneous throughout the matrix.

To better characterize the γ' phase, TEM micrographs were taken of the initial microstructures, Figures 10-11. Gamma prime precipitate sizes are seen to be approximately 0.08 μm for each alloy of the S series and 0.6 μm for the L series. Higher magnification dark field images reveal the presence of hyperfine γ' particles in all alloys with an average size of 0.008 μm. The γ' morphology ranges from spherical in alloy 2, the low mismatch alloy, to a blocky form in the larger mismatch system. Such morphologies are entirely consistent with basic physical metallurgy principles. In the untested condition, the dislocation density is seen to be very low. Only isolated dislocations, which were probably generated during forging and machining, are present in all of the alloys.

4.2 Microstructural Property Measurements

4.2.1 Anti-Phase Boundary Energy

APBE values for each alloy and γ' size are listed in Table II. These values were determined using the spacing of superpartial dislocations as described previously (eq. 14). As shown in Table II, the APBE was not significantly altered as the γ' size was increased from 0.08 μm to 0.5 μm. In each case alloys 1-3 have a value of about 75 ergs/cm^2, while alloy 4 is 140 ergs/cm^2. For ease of presentation alloys 1-3 are considered to have a "low" APBE and alloy 4 has a "high" APBE.

4.2.2 Mismatch

Mismatch values are summarized in Table II for each alloy system. In each alloy the γ' had a larger lattice parameter and thus a positive value for δ. Again, as for the APBE, the alloys will be classified as having high, medium or low mismatch. Alloy 3 is considered to have high mismatch and alloy 4 to have medium mismatch.

4.2.3 Volume Fraction of γ'

Volume fraction determination seems at first to be a simple parameter to measure. However, many inaccuracies are inherent in the measurement techniques resulting in some degree of uncertainty in the values. Volume fraction determinations in the TEM require a correction to account for the three dimensional nature of the foil. This requires a knowledge of the foil thickness which is difficult to determine. Phase extraction allows very small particles to pass through the filter paper and thus are not accounted for in the measurement of the extracted γ' phase weight. Finally measurements using optical micrographs require assumptions in the distribution of the phase through the thickness when using stereological equations. The values reported in Table II represent an average of all three techniques. Any value which deviated significantly from the other three techniques was discarded. Still, it is likely that the values reported are slightly lower than the actual value due to the

difficulties associated with measuring the very small sizes present in all four alloys.

Since the large γ' materials also contain some very small γ' precipitates the volume fraction represents contributions both from the large and small particles. Use of stereological equations on TEM micrographs indicate that approximately 70% of the total volume fraction reported in Table II for the L series alloys is accounted for by the large precipitates.

4.3 Monotonic Properties

True stress-strain curves for all alloys in this study are shown in Figure 12 with the monotonic properties summarized in Table II. It is immediately apparent that alloys 2-4 have similar mechanical properties while alloy 1 has a much lower yield stress and ultimate strength due primarily to the very low volume fraction of $\gamma'$and the low values of δ and APBE. Yield stress values for each alloy are qualitatively consistent with those predicted from the deformation models. According to equation 4, the flow stress should increase with misfit due to the increased strain field surrounding the precipitate. This strain field interacts with a mobile dislocation and is a barrier to continued motion. Equation 5 predicts an increase in CRSS resulting from an increase of APBE when particle shearing occurs. Finally, for alloys which deform by particle shearing, an increase in precipitate size will increase the flow stress. Above some critical value of particle radius, dislocation bowing will occur

and an associated drop in flow stress with precipitate size will occur.

Series 1 alloys have low APBE, low δ, and low V_f. Based on the preceding information this system would be expected to have the lowest yield strength. In fact series 1 has approximately half the yield strength of the other alloys. Conversely, alloys 3 and 4 have relatively high volume fractions and either a high APBE (alloy 4) or high δ (alloy 3) and possess the largest yield strengths. Alloy 2 has a high V_f but low APBE and low δ and, as expected, falls between series 1 and 3-4 in terms of yield strength.

Most FCP models predict an inverse relationship between crack growth rate and yield strength (e.g. equations 9 and 11). On this basis alone microstructural effects on FCP properties for alloys 2-4 can be directly and unambiguously examined without the complicating effect of different strength levels. With all other factors constant, one would expect alloy number 1 to show a much higher FCP rate due to the low strength. It is therefore useful to attempt to normalize the FCP results with respect to yield strength thereby eliminating the differences in strength.

The effect of increasing the γ' size was to slightly increase both the yield and ultimate strengths of all alloys while slightly decreasing their ductility.

4.4 Fatigue Crack Propagation

In Figure 13, the FCP response of the small γ' alloys tested at an R-ratio of 0.1 at room temperature in air is presented. Correlation of FCP rates as a function of ΔK describes a materials response to cyclic loading. Crack extension at a given value of ΔK is a function of both the amount of damage imposed on the specimen and the material's intrinsic ability to accommodate the damage. For a given stress level, an alloy with a low yield stress but high resistance to crack extension can exhibit the same FCP rate as an alloy with a high yield strength and low crack growth resistance. Since series 1 alloys have a much lower yield strength, the FCP response represented in Figure 13 can be misleading. At a given level of ΔK alloy 1 will experience a greater amount of plastic deformation at the crack tip due to the lower yield stress. More damage is therefore occurring at crack tip of the series 1 alloy. However, it has a comparable FCP rate to the other alloys. Series 1 alloys can therefore accommodate a larger amount damage before crack extension and are intrinsically more resistant to crack extension at equivalent amounts of crack tip plasticity. It therefore becomes meaningful to normalize the data in terms of the damage imposed at the crack tip.

The exact form of the normalization is a matter of debate. It would be necessary to assume a model of damage accumulation to arrive at an exact form of the normalization. A straight-forward technique is to normalize with respect to plastic strain at the

crack tip based on an elastic plastic solution for crack tip stress and strain. The form is as follows;

$$\frac{\Delta K}{a(\sigma_{ys}E)^{b}} \quad . \quad . \quad . \quad (13)$$

where the constants a and b depend on the model chosen. Since no consensus exists concerning which model is correct a and b will be chosen as 1. Since the series 1 alloys is the only one with a significant difference in tensile properties the exact values of a and b will only affect the relative position of alloy 1's FCP curve. Further, since the difference in alloy 1's yield strength is significantly larger than the others, the differences due to other values of a and b are further reduced. The FCP curves normalized to yield strength and modulus are shown in Figure 14.

Roughness measurements of the fracture surfaces shown in Figure 15 as a function of ΔK are presented in Figure 16. Comparison of these results with Figure 14 shows that the specimen with the largest fracture surface roughness has the greatest resistance to crack growth while the specimen with a relatively smooth fracture surface has the highest growth rate. Initially this seems to imply that FCP is controlled by a roughness induced closure effect (this will be discussed later).Examination of the fracture surface, Figure 18, shows that roughness of the fracture surface is due to cracking along slip bands which formed in the material.

4.4.1 Closure

The question arises as to the mechanism for the improved FCP resistance of the series 2 alloys. Micromechanical theories would explain this improved resistance in terms of the ease of dislocation motion, which is possible in planar slip materials, resulting in less damage accumulation. Closure proponents would attribute the improvement in life to crack tip shielding due to mechanical locking of the fracture surface asperities. To address these issues, closure measurements were performed using the laser exstensometer during the course of the test.

Figure 17 shows an optical micrograph of the fracture surface corresponding to a ΔK level of 16.5 MPa$\sqrt{m}$ (15 ksi$\sqrt{in}$). The roughness parameter at this ΔK level was measured to be 1.6. Specimens with an identical composition and heat treatment were used in evaluating the different closure measurement techniques due to the large surface roughness which resulted. It is expected that the large asperity height in these specimens will promote a situation in which roughness induced closure occurs. This provided an opportunity to compare the closure loads measured with the laser extensometer to the BFSG and clip gage.

Figure 18 shows a schematic load vs. displacement curve commonly used in determining closure. The closure load is found from the intersection of the two linear segments of the curve. As a comparison, the results from the three techniques used in the present study are shown in Figure 19. The curves corresponding to

each technique in Figure 19 are similar to the curve in Figure 18. It is common practice to measure closure loads using both the clip gage and BFSG. Agreement between the different techniques is one criterion often used to establish the reliability of the measured closure load. For the present case, the clip gage and laser extensometer produce similar results while the BFSG is approximately 5% lower. The differences are within the limits of experimental error, thus an average value calculated from the three curves could be used as a measure of the closure load. However, the curves in Figure 19 were obtained from a specimen with no crack, only the machined notch! Clearly no closure mechanism can operate when there is no crack. (The loads used were sufficiently low to insure no gross plasticity was present which would result in non-linear displacement behavior.) These curves indicate that closure occurred at approximately 40% of P_{max} which would reduce K_{eff} substantially, if closure was indeed occurring. It is important to note that each curve has a finite amount of curvature at all points and no clearly linear region exists even at loads greater than the apparent closure load. The curvature in this case is simply an artifact of the testing procedure and must be eliminated before proceeding.

The similarity in the curves is striking. This comparison of the cracked and uncracked specimens demonstrates that closure measurements are not a trivial matter. It is possible to measure an apparent closure load from a load-displacement/strain graph where the non-linearity is due to reasons other than closure. It

is important to note that our technique for alignment, gage linearity, etc met or exceeded all present ASTM requirements. Also, use of more than one measurement technique to confirm the validity of the closure load determination is seen to be an insufficient criteria. Since the influence of closure on FCP rates is currently an area of intense interest, the first step of any program investigating this effect must be to ensure that the closure measurements are accurate and reproducible. All errors inherent to the measurement technique used must be fully appreciated and accounted for.

Poor machine alignment was initially suspected as the source of the non-linearity. Alignment was found to be acceptable by current standards but further refinements were made. When testing at low R ratios and low loads the minimum load can be very near zero; thus any freedom of motion in the load train will result in non-linear load-displacement behavior. Unfortunately, low R ratios are where closure is expected to be most significant since the crack opening displacement (COD) is relatively small. To minimize this possible source of error, the cross head was lowered such that load transfer system was as short as possible and the force rods were stiffened at both ends by locking rings. Additionally, pins with a smaller diameter than the specimen holes were used to reduce friction in the clevis assembly which could affect the displacement reading during loading.

The load-displacement curve using the laser extensometer for the uncracked specimen obtained after performing the above

modifications is shown in Figure 20. The BFSG and clip gage continued to exhibit non-linear behavior whereas the laser system was linear over the entire load range. The laser gave constant compliance recordings as long as the load frame was undisturbed. Repeated specimen insertion and removal had no effect on the subsequent output as seen by the four curves in Figure 20. However, if for instance the lower clevis was rotated 180^{o} from the initial position in which the machine was aligned the non-linear output from the laser extensometer for the uncracked specimen reappeared. Even if the clevis was initially machined perfectly, after repeated use over the course of several years some amount of distortion in the clevis would be expected. This distortion is reflected in the non-linear behavior of subsequent compliance readings. It is therefore imperative that the testing machine be initially aligned precisely and left undisturbed as much as possible. Any change in the system can possibly affect alignment and make interpretation of the data subject to error. The final and most important evaluation as to the reliability of the testing procedure is the consistently linear behavior of an elastically loaded uncracked specimen.

The clip gage gave inconsistent results. If it was removed and replaced on the specimen, a linear displacement output could be obtained in most cases during loading and unloading. This however was not reproducible nor could the response be predicted before-hand. In some cases once the clip gage was removed and replaced, non-linear behavior was observed. Since the gage was

resting on knife edges the positioning of the gage was critical. Any slippage or transverse rotations of the gage will affect the output.

The BFSG never gave a linear output. Once an installed strain gage is connected to a strain indicator and the instrument is balanced, a change in the temperature of the gage will generally produce a resistance change in the gage. Because this temperature-induced resistance change in the gage will be registered by the strain indicator as strain, the indication is referred to as apparent strain. The apparent strain caused by the temperature change is potentially the most serious error source in strain measurement [39]. It was possible, over the course of several seconds, to record significant variations in the strain level even while the specimen was held at a constant load. Temperature changes caused by lab air conditioners and self heating of the gage from the applied current all contribute to this fluctuation in strain. Since compliance readings are generally taken at a frequency of about 1 Hz this drift in strain can contribute to non-linearity of the compliance curve as was observed.

There are many procedures which can be taken to reduce the temperature induced drift in strain. For instance, the apparent strain can theoretically be completely eliminated by employing, in addition to the active strain gage, an identical compensating or "dummy" gage. This compensating gage should be mounted on an unstrained portion of the specimen and will exactly balance the

apparent strain due to temperature fluctuations. This will leave only the stress induced strain in the active strain gage to be registered by the strain indicator [39]. This technique was successfully employed in this study to eliminate the temperature induced changes in strain while under constant load. However, after eliminating the temperature induced strain readings the load-strain output was still slightly non-linear over the entire loading cycle, resulting in unreliable closure load determinations.

The next phase of the project was to measure closure during an FCP test. It was a relatively simple matter to obtain consistent results from the laser extensometer once machine alignment was acquired and a stable load train system was put in place. Closure measurements on the cracked specimens were therefore recorded by the laser extensometer exclusively and are described below. This does not imply that closure measurements obtained by other means are less accurate. The clip gage and back face strain gage can theoretically provide essentially the same information as long as their potential errors are understood and corrected. Clip or strain gages however are more prone to error and in addition require some specimen preparation such as machining grooves, applying knife edges, or gluing strain gages.

Compliance measurements of a CT specimen with a crack grown to a ΔK level of 16.5 MPa$\sqrt{m}$(15 ksi$\sqrt{in}$) produced the curve shown in Figure 21. This curve possesses features which are essential to a true indication of closure. Namely, the plot consists of a

linear upper segment with a slightly curvilinear lower segment where crack face contact is occurring. In the region where no fracture face contact is present (region II in Figure 6) any non-linearity, as in Figures 18 and 19, is unacceptable. Curvature near P_{max} is not due to closure unless region II is absent (i.e. $P_{cl} \sim P_{max}$) in which case there is nearly 100% closure. Curvature in the load-displacement plot in this region is possible only if there is crack tearing or gross plasticity. If region II possess non-linearity some mechanism other than closure is operating and must be identified and/or eliminated. Region I in Figure 6. represents crack face contact. In the case of an incompressable particle wedging the crack open or crack closure due to plasticity, a linear region should exist. If roughness induced closure is operating a non-linear response would be expected as the asperities rub together and result in varying amounts of load shedding.

As the distance from the crack tip is decreased the change in compliance due to closure is increased. The value for P_{cl} was decreased slightly for decreasing values of X (Figure 7) at a constant K. Since the change in compliance due to closure is more pronounced at smaller values of X, it is likely that load line clip gage measurements of closure loads are more accurate than those obtained from the front face. This increased accuracy is a result of the greater change in slope associated with the onset of closure when measured closer to the crack tip. It is counterbalanced, of course, by the experimental difficulties

previously mentioned.

Measured closure loads for R = 0.1 are shown in Table III. From the closure load data it is possible to compute ΔK_{eff} and use it to correlate the dadN data. Using ΔK_{eff} resulted in little change of the dadN as seen in Figure 22. The closure load was always less than 15% of P_{max} and did little to influence the data. Although there was a significant difference in fracture surface roughness between the four alloys, there was little difference in the amount of closure measured during the FCP test. Alloy 4S had a nearly flat fracture surface ($R_f \cong 1$) and exhibited closure loads of about $0.08P_{max}$ while specimen 2S had a very tortuous fracture path ($R_f \cong 1.6$) although the closure load was only slightly higher ($\sim 0.12P_{max}$).

Due to the inaccuracies of any current closure measurement technique and the desire to account for closure as completely as possible, the FCP tests were repeated for all alloys at an R-ratio of 0.8. At high R-ratios the height of the crack face asperities are much smaller than the crack tip opening displacements thus eliminating any roughness effects. The results are shown in Figures 23-24. The high R-ratio tests had no measurable crack closure over the entire range of ΔK tested. This implies that plasticity induced closure did not play a role in this study since at high R-ratios (high mean stress) plasticity effects should be most pronounced.

As with the ΔK_{eff} results, the ranking of data is unaffected

at the high R-ratio although the absolute value of dadN at R = 0.8 is higher due the larger mean stress. It is clear that the observed differences in growth rates for these alloys are due to some micromechanical process and not an "extrinsic" effect such as closure as is often cited. With all external factors eliminated it is now possible to identify the dominate features controlling the FCP rates.

4.4.2 Deformation Structures

4.4.2.1 Small γ' Alloys

Transmission electron micrographs of alloys 2 and 4 (Figure 25) reveal quite different deformation mechanisms. Due to the small size of the precipitates, dislocation shearing is the predicted deformation mode and (Figure 4). However, as Figure 25 shows, while alloy 1S,2S, and 3S consist of dislocations in well defined slip planes, in alloy 4S deformation is accomplished by dislocations looping around the precipitates. For shearing to occur the stress to shear a particle (eq. 1) must be less than the Orowan looping stress (eq 2.) In the case of alloy 4S, the APBE is sufficiently high as to prevent shearing even in the presence of very small γ' particles.

Examination of the deformation structures in alloy 2 and 4 suggests a serious problem which must be accounted for when modeling the FCP process. Specifically, any proposed model must account for different deformation modes depending on the specific

alloy system and test conditions. Those factors which are important in controlling FCP when the precipitates are sheared, for example, may not operate when dislocation by-pass occurs. A single closed form fundamental model to predict FCP rates therefore seems unlikely. A more reasonable solution would be to model the individual processes which occur in a specific alloy system and identify under what conditions specific solutions are applicable.

4.4.2.2 Large γ' Alloys

The deformation structures for the large γ' alloys are shown in Figure 26. The structures in each case consist of large (~ 0.6 μm) γ' particles in addition to very small hyperfine (~0.008 μm) particles which probably formed during cooling. This bimodal size distribution of precipitates produces a mixed deformation structure. The hyperfine γ' precipitates promote particle shearing by dislocations in well defined slip bands in addition to dislocation by-pass of the large γ' particles (Figure 27). In some cases (Figure 28), slip bands intersect with a large γ' particle thereby shearing it and the APB created during the process resists deformation.

4.4.3 FCP of Small γ' alloys

4.4.3.1 Effect of V_f

From the da/dN vs. ΔK plots (Figures 14 and 24) it is clear that alloy 1S (low Γ, low δ, low V_f) is most resistant to crack advance. When normalized as described above, the FCP rate of this alloy system is at least two orders of magnitude slower as compared to the others. The low volume fraction of precipitates results in a larger mean free path between obstacles for the mobile dislocations. The imposed plastic strain is therefore more easily accommodated resulting in less damage accumulation and thus greater resistance to crack advance. The efficiency of the γ' as obstacles to dislocation motion is reduced further in this alloy by the low vales of APBE and δ as described by equations 4 and 5. Conversely, alloy 2S has the same APBE and δ but a much higher V_f of γ'. This combination results in relatively higher crack growth rates. The ability of this material to accommodate strain at the crack tip is reduced by small mean free path of the dislocations.

4.4.3.2 Effect of APBE

The decreased resistance to FCP due to higher APBE (alloy 4S) is due to the difference in deformation mode caused by the APBE. In the other S series alloys, which have various combinations of APBE and V_f, particle shearing occurs, Figure 25, whereas for alloy 4S with a high APBE particle by-pass is the

dominant deformation mode. Since dislocation looping occurs the motion of dislocations does not create APB and thus no increase in energy results. Rather, the increased APBE prevents dislocations from entering the precipitate and forces them to by-pass the particle. With particle looping, the contribution of δ toward inhibiting dislocation motion is even more pronounced since in the looping regime the CRSS is directly related to mismatch by equation 4.

This effect is similar to the results obtained by Antolovich et. al [25] where it was observed that increasing the stacking fault energy reduced the FCP resistance. The increased stacking fault energy promoted cross-slip of dislocations (non-planar deformation) resulting in more dislocation tangles and thus greater accommodation of damage.

4.4.3.3 Effect of Mismatch

In the case of small γ' precipitates alloy 2S and 3S have a difference of 3-5 times in FCP rates due only to changes in mismatch and a slight difference in V_f. In fact, from the previous argument, increased V_f is seen to increase the FCP rate when normalized with respect to σ_{ys} and E due to a lowering of the mean free path. All other factors being constant, a lower volume fraction of precipitates should reduce the FCP rate. Therefore, the differences in alloys 2S and 3S FCP response is even greater if alloy 2S is shifted down in the FCP plot (or 3S is shifted up) to account for the difference in mean free path.

The increase in FCP rate for the higher mismatch alloy is a result of the increased resistance to dislocation motion due to the enhanced strain field around the precipitate and/or a different deformation mode.

4.4.4 FCP of Large γ' alloys

Fatigue crack propagation response for series L alloys is shown in Figures 29-32. The response of these alloys is very similar to the S series results even though 70% of the γ' volume fraction is accounted for by the large (> 0.5 μm) particles. It is clear that the presence of the hyperfine γ' particles is significant in controlling the FCP rates in these alloys in that the dislocations are restricted for the most part to slip bands even in the presence of the large particles.

The most notable difference in FCP response between the S and L series alloys is seen in alloy 4. In the S series this alloy had a FCP rate much faster (~ 50 times), Figure 14, than the next closest whereas in the L series the difference is reduced to about 20 times, Figure 30. In the S series, alloy 4 had a different deformation mode (looping) and thus a much greater FCP rate for the reasons previously discussed. In the L series, each alloy deforms in a similar manner (i.e. a combination of looping and shearing) leaving only the intrinsic microstructural factors to control the FCP rates.

The trends concerning the effects of APBE, δ, and V_f on FCP rates for the small γ' material are followed in the L series as

well. The overall FCP rates for the L series alloys is in each case slightly lower than that of the S series. For a constant γ' V_f, coarsening of the γ' (L series) results in a larger mean free path for the dislocations thus allowing the strain to be more easily accommodated thus accumulating less damage and increasing the FCP resistance.

5. SUMMARY

The investigation summarized in this report lead to information concerning the effects of microstructure on the fatigue crack propagation response of nickel-base superalloys. Among the variables studied were volume fraction of γ', lattice mismatch, and anti-phase boundary energy. In addition, precipitate size was varied through heat-treatment.

Fatigue crack propagation tests were conducted in lab air at room temperature under constant load (increasing K) conditions with a stress ratio of 0.1. To account for crack tip shielding, crack closure loads were measured with a laser extensometer, front face clip gage, and a back face strain gage. Also, tests were run at a high R-ratio (R = 0.8) to eliminate any roughness induced closure effects.

The constant load tests were performed on each of four alloy compositions with two different γ' sizes to characterize the steady state FCP response of these alloys. The following observations can be made about the constant load FCP behavior of these alloys:

MECHANISMS

1) Crack closure concepts do not explain differences in the FCP rates for both near threshold and Paris regime propagation in the model Ni base alloys studied here.

2) FCP rates are dramatically low for those compositions and treatments that promote planar, reversible slip.

3) In this study, alloys having high volume fraction, low APBE, and low mismatch exhibited FCP rates that were approximately fifty times lower than other treatments.

4) Internal resistance to damage ahead of a crack is achieved by low volume fraction of precipitates, low lattice mismatch, and low anti-phase boundary energy. FCP resistance is increased by a planar deformation mode. However, in a planar slip material, on a strength/modulus normalized basis, restricting dislocation motion decreases the alloy's ability to accommodate damage and consequently further decreases the FCP rate.

5) At the same strength level, it has been demonstrated that the FCP rate can be varied by approximately 50 times.

6) Changes in deformation mode and consequently damage accumulation mechanisms hinders development of a global, closed form fundamental model of FCP rates in Ni base alloys.

CLOSURE MECHANISMS

1) Closure measurements require excellent test machine alignment and are very sensitive to changes in the testing equipment.

2) Use of more than one closure measurement technique is insufficient to establish the validity of the procedure. Use of an uncracked specimen to calibrate the measurement procedures insures that any non-linearity of the compliance output is not an artifact of the test equipment.

3) Properly measured closure loads were much lower than previously reported for similar alloy systems.

IMPROVED FCP RESISTANCE IN NI-BASE ALLOYS

These studies have shown that FCP rates can be reduced dramatically by the following means:

1. Lower mismatch (moderate effect) - chemistry
2. Lower APBE (strong effect) - chemistry
3. Lower volume fraction (strong effect but results in loss of strength) - chemistry
4. Decrease precipitate size (strong effect) - heat treatment

Such procedures can be carried out by small modifications of existing alloys and changes in heat treatments.

REFERENCES

1. R.J. Hill, W.H. Reimann, and J.S. Ospey, A Retirement-for-Cause Study of an Engine Turbine D1512, AFWAL-TR-81-2094, Air Force Wright Aeronautical Laboratories, 1981.

2. C.T. Sims and W. C. Hagel, The Superalloys, John-Wiley and Sons, Inc., New York, 1979.

3. P.A. Flinn, Trans. AIME, Vol. 218, 1960.

4. R.G. Davies and N.S. Stoloff, Trans. AIME, Vol. 233, 1965.

5. T.L. Johnston, A.J. McEvily, and A.S. Tetelman, in High Strength Materials, V.F. Zackay ed., John-Wiley and Sons, Inc., New York, 1965.

6. S.M. Copley and B.H. Kear, Trans. AIME, Vol. 239, 1967.

7. P.H. Thorton, R.G. Davies, and T.L. Johnston, Metall. Trans., Vol 1, 1970.

8. C. Lall, S. Chin, and D.P. Pope, Metall. Trans., Vol. 10A, 1979.

9. E. Kuramoto and D.P. Pope, Acta Metall., Vol. 21, 1978.

10. K. Aoki and O. Izumi, Acta Metall., Vol. 26, 1978.

11. S.S. Ezz, D.P. Pope, and V. Paidar, Acta Metall., Vol. 30, 1982.

12. B.H. Kear and H.G.f. Wilsdorf Trans. AIME, Vol. 224, 1962.

13. R.K. Ham, Ordered Alloys: Structural Applications and Physical Metallurgy, Claitors, Baton Rouge, Louisiana, 1970.

14. E. Orowan, "Symposium on Internal Stresses in Metals," Institute of Metals, London, 1948.

15. D.P. Pope and J.L. Garin, J. Appl. Crystallogr., Vol. 10, 1977.

16. V. Gerold and H. Haberkorn, Phys. Stat. Sol., Vol. 16, 1966.

17. S.M. Copley and B.H. Kear, Trans. Met. Soc. AIME, Vol. 239, 1967.

18. G.R Leverant, M. Gell, and S.W. Hopkins, Proc. Second Int. Conf. Strength of Met. Alloys, Vol. 3, 1970.

REFERENCES

19. A. Saxena and S.D. Antolovich, Metall. Trans., Vol. 6A, 1975.

20. B. Lawless, M.S. Thesis, University of Cincinnati, Cincinnati, Ohio, School of Materials Engineering, 1980.

21. D.D. Krueger, S.D. Antolovich, and R.H. Van Stone, Metall. Trans., Vol. 18A, 1987.

22. J. Gayda and R.V. Miner, Metall. Trans., Vol. 14A, 1983.

23. J.K. Shang, J-L Tzou, and R.O. Ritchie, Metall. Trans., Vol. 18A, 1987.

24. B. Lawless, S.D. Antolovich, C. Bathias, and B. Boursier, Fracture: Interactions of Microstructure, Mechanisms, Mechanics, J.M. Wells and I.D. Landes, eds., TMS-AIME, Warrendale, PA, 1984.

25. S.D. Antolovich, A. Saxena, and G.R. Chanani, Eng. Frac. Mech., Vol. 7, 1975.

26. G.T. Gray, A.W. Thompson, J.C. Williams, and D.H. Stone, Fatigue Thresholds, J. Backland, A. Blom, and C.J. Beevers, eds., EMAS Publ. Ltd., Warley, U.K., 1981.

27. J.L. Yuen, Ph.D. Thesis, Stanford University, Stanford, CA., 1982.

28. R.O. Ritchie and S. Suresh, Metall. Trans., Vol. 13A, 1982.

29. W. Elber, Eng. Fract. Mech., Vol. 2, 1970.

30. R.O. Ritchie, S. Suresh, and C.M. Moss, J. Eng. Mater. Technol., Vol. 102, 1980.

31. R.O. Ritchie, Fatigue Thresholds, J. Backland, A. Blom, and C.J. Beevers, eds., EMAS Publ. Ltd., Warley, U.K., 1981.

32. P. Paris and F. Erdogan, J. of Basic Eng, Trans. ASME, Series D, Vol 85, 1963.

33. A.G. Forman, J. of Basic Eng., Vol. 89, 1967.

34. J. Weertman, "Fatigue Crack Propagation Theories," in Fatigue and Microstructures, ASM, Metals Park, Ohio, 1979.

REFERENCES

35. J.P. Bailon and S.D. Antolovich, Fatigue Mechanisms: Advances in Quantitative Measurement of Physical Damage, ASTM STP 811, J. Lankford, D.L. Davidson, W.L. Morris, and R.P. Wei, eds., ASTM, 1983.

36. R.F. Miller and G.S. Ansell, Metall. Trans., Vol. 8A, 1977.

37. E.E. Underwood, Quantitative Stereology, Addison-Wesley Pub. Co., Reading Mass., 1978.

38. C.F. Richards and W.F. Dean, The Measurement of Crack Length and Shape During Fracture and Fatigue, EMAS Publ., Ltd., West Midlands, U.K., 1980.

39. D.L. Davidson and A. Nagy, J. Phys. E. Sci. Instrom., Vol. 11, 1978.

40. K. Banerji, Ph.D. Thesis, Georgia Institute of Technology, School of Materials Engineering, Atlanta, Georgia, 1986.

PUBLICATIONS, PRESENTATIONS AND INTERACTIONS

I. Publications

1. R. Bowman and S.D. Antolovich, "Microstructure and Stability of Melt-Spun IN718", Metall. Trans., Vol. 17A, 1986, pp. 173-180.

2. R. Bowman and S.D. Antolovich, "Effect of Melt-Spinning on the Microstructure and Mechanical Properties of Three Ni-Base Superalloys", Metall. Trans., to appear early 1988.

3. R. Bowman and S.D. Antolovich, "Problems associated with Closure Load Determinations," Eng. Fract. Mech., in press.

4. "Microstructure and Deformation Mode on Constitutive Behavior, Low Cycle Fatigue and Fatigue Crack Propagation of Ni Base Superalloys", Invited paper to be presented at International Meeting on Constitutive Behavior and Fracture, Ottawa, Canada, 1989.

5. "Control of FCP rates Through Microstructural Control", To be submitted for Sixth Annual Symposium on Superalloys, Seven Springs Mountain Resort, Champion, Pennsylvania.

6. R. Bowman and S.D. Antolovich, "The Effect of Microstructure on the Fatigue Crack Growth Resistance of Ni-Base Superalloys", in preparation for submission to Metall. Trans.

II. Presentations

1. R. Bowman, "Microstructure and Stability of Melt-Spun IN718", AIME Annual Meeting, 1983.

2. R. Bowman, "Effect of Melt-Spinning on the Microstructure and Mechanical Properties of Three Ni-Base Superalloys", TMS-AIME Annual Meeting, 1986.

3. S.D. Antolovich, Seminar presented to Sandia Laboratories, Feb. 1987.

4. S.D. Antolovich, Seminar presented to the Albuquerque ASM chapter, Feb. 1987.

III. Interactions

1. Wyman-Gordon Corporation
Mr. Red Couts and Steve Reichman generously agreed to process the materials thereby obtaining uniform grain sizes and compositions.

2. South West Research Institute
Numerous discussions have been held with Dr. David Davidson about measurement of strain distributions around the crack tip. At one point it was anticipated that specimens would be fabricated and tested in the SWRI in-situ SEM loading stage to obtain some idea of closure and strain levels at the crack tip. To date this has not been done since we found other means to measure closure levels. It is still anticipated that some work to measure or confirm strain levels will be done after this project officially terminates.

3. University of California, Berkeley
Numerous discussions have been held with R.O Ritchie about effects such as the difference of philosophy and different opinions on the importance of closure for Ni base alloys.

4. Air Force Materials Lab
The principal investigator has served on the Ph.D. thesis committee of Dr. Larson and plans detailed discussions of the results with Dr. Nicholas.

III. Personnel

All those who have participated on the project are listed below;

NAME	FUNCTION
1. Stephen D. Antolovich	Principal Investigator
2. Randy Bowman	Ph.D. graduate student. carried out bulk of experimental work and is in process of writing Ph.D. dissertation.
3. Brad Lerch	Post-doctoral fellow. Helped in interpretation analysis and testing.

4. Rick Brown	Technician in FFRL. Helped with testing and design of some experiments.
5. Pete Noel	Machinist shared by Ch.E.-FFRL - Mat.E. Mr. Noel machined some fixtures and grips.
6. Pat Ledon	Senior administration secretary. Ms. Ledon helped in preparation of papers and with some of the administrative aspects of the project.
7. Others	Some assistance was obtained from secretaries and technicians in the School of Materials Engineering.

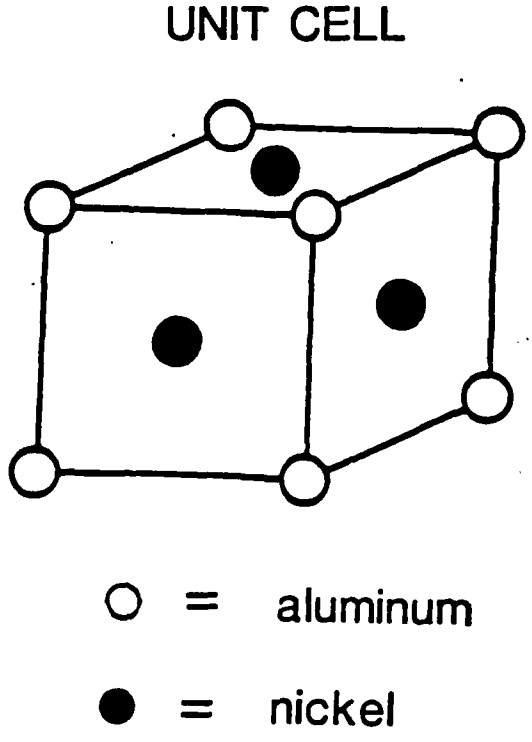

Fig. 1 - Ordered gamma prime unit cell has a face centered cubic ($L1_2$) structure with aluminum atoms at the corners and nickel atoms on the face centers.

mismatch = 0.07%

mismatch = 0.21%

Fig. 2 - TEM micrograph of experimental nickel base superalloy showing effect of lattice mismatch on γ' morphology.

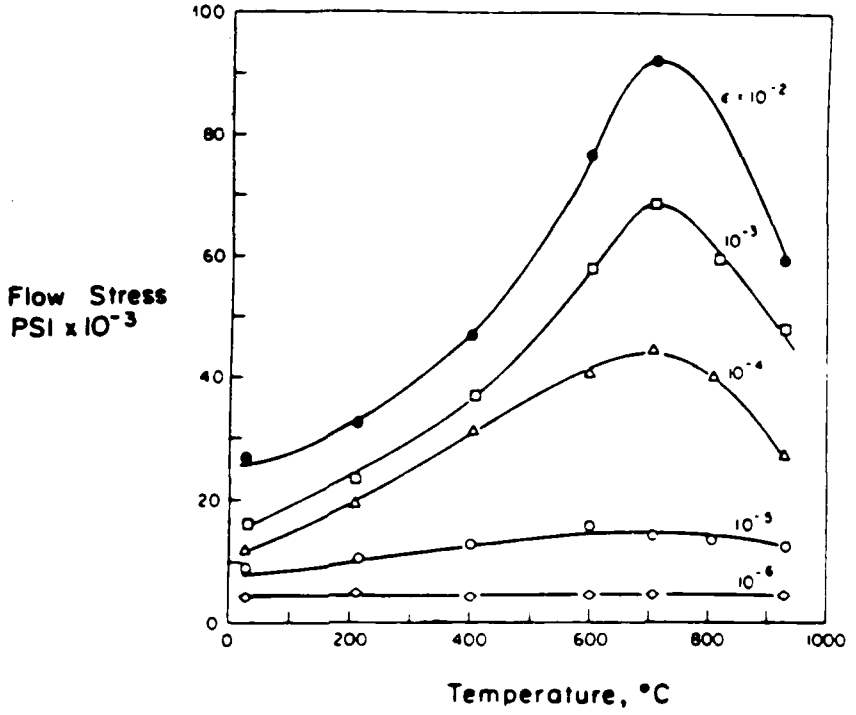

Fig. 3 - Rise in flow stress of γ' with temperature, measured at various strain (ε) levels [2].

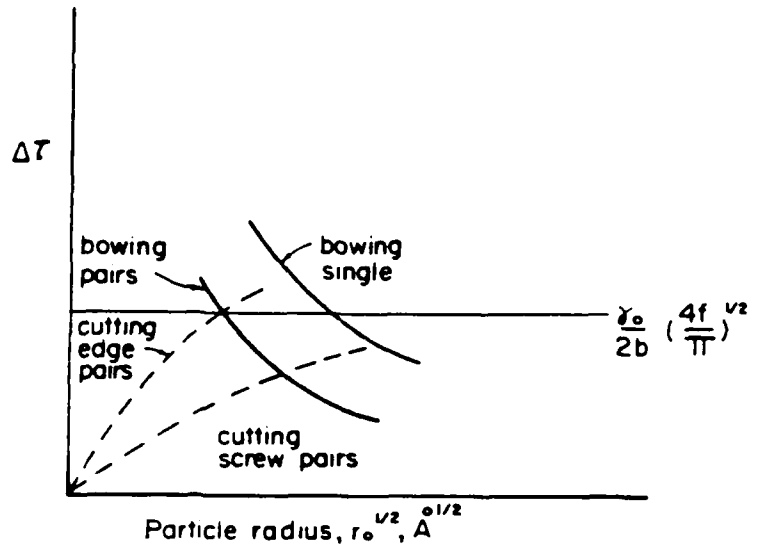

Fig. 4 - Schematic of age hardening curves illustrating relation between order strengthening and Orowan bowing as a function of particle size [2].

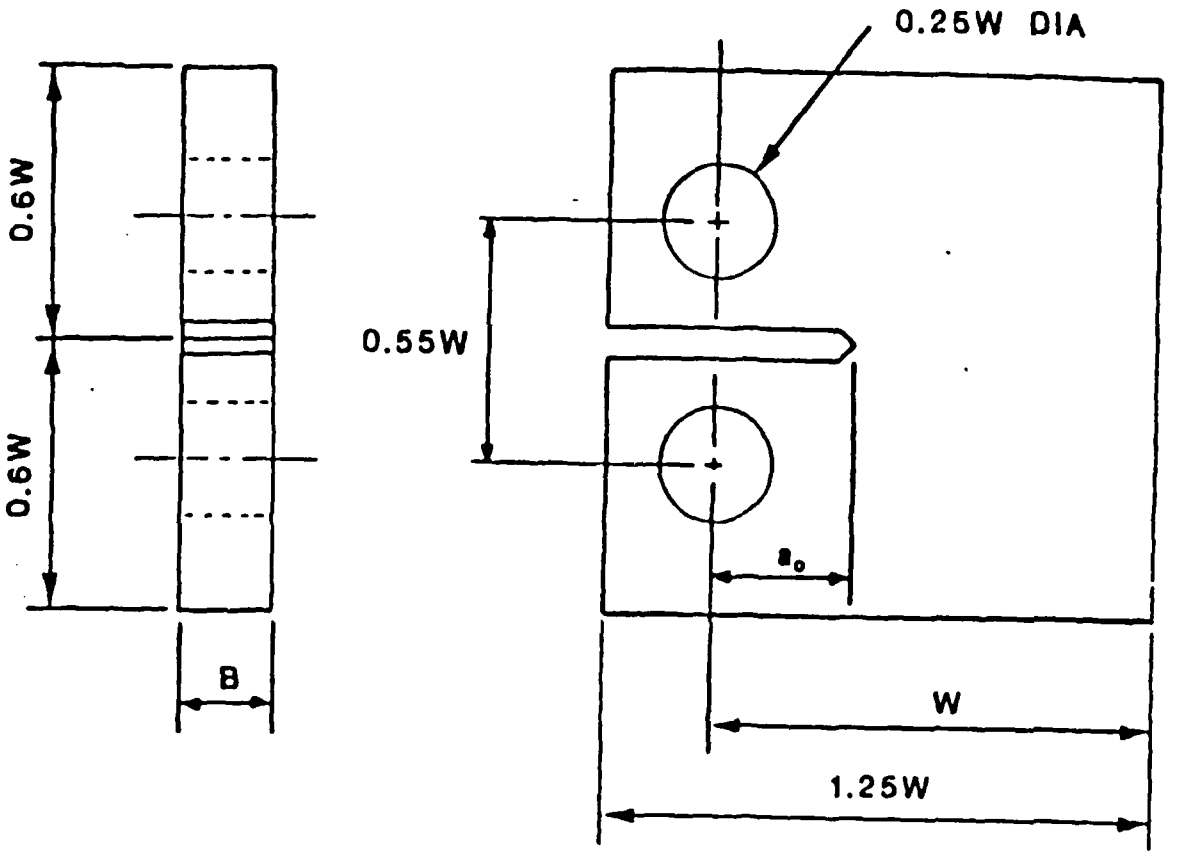

W = 1.500"
a_o = 0.3 W
B = 0.186"

Fig. 5 - Standard ASTM fatigue crack propagation specimen.

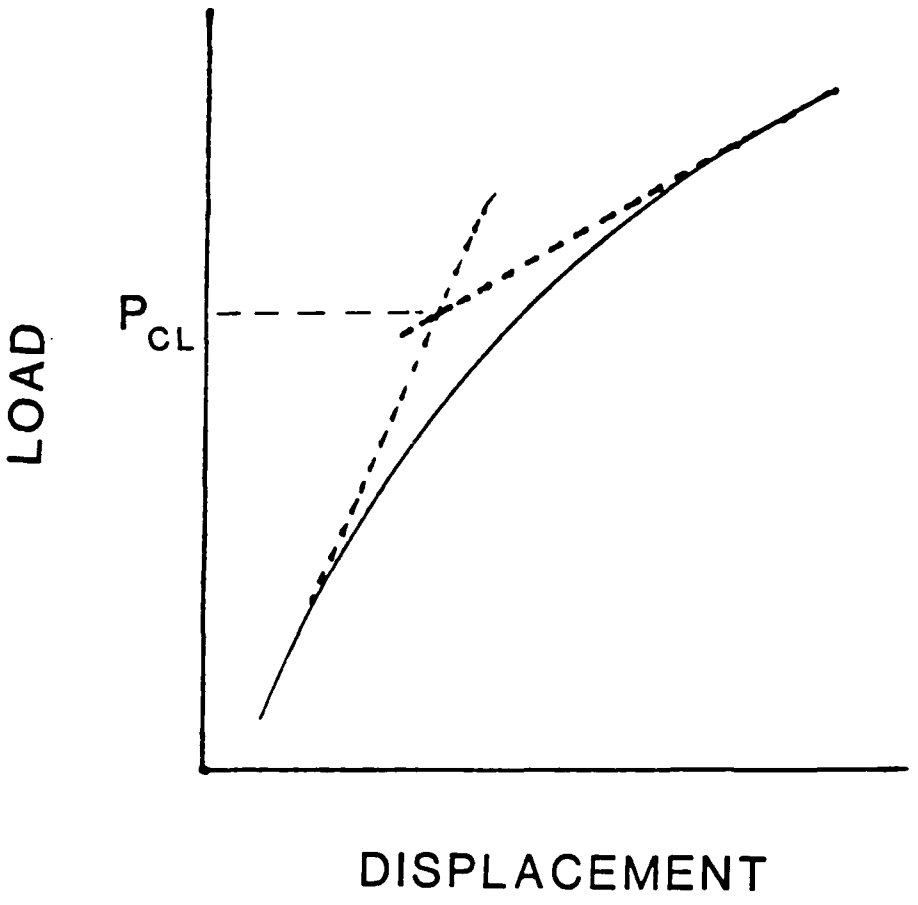

Fig. 6 - Schematic compliance curve illustrating change in slope due to closure phenomena.

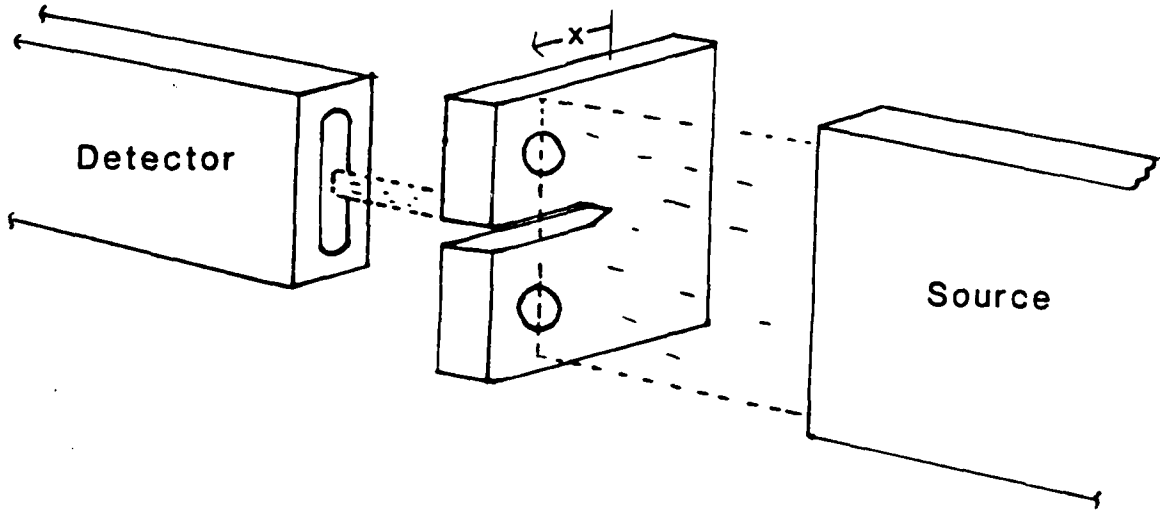

Fig. 7 - Laser extensometer used to measure specimen displacements.

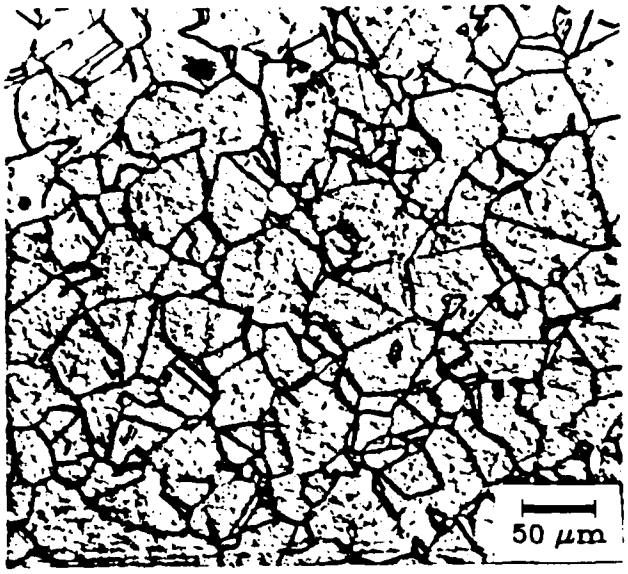

alloy 1s

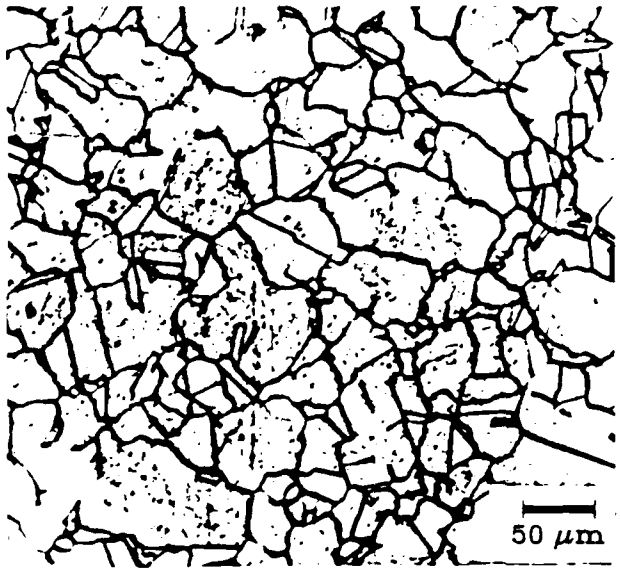

alloy 2S

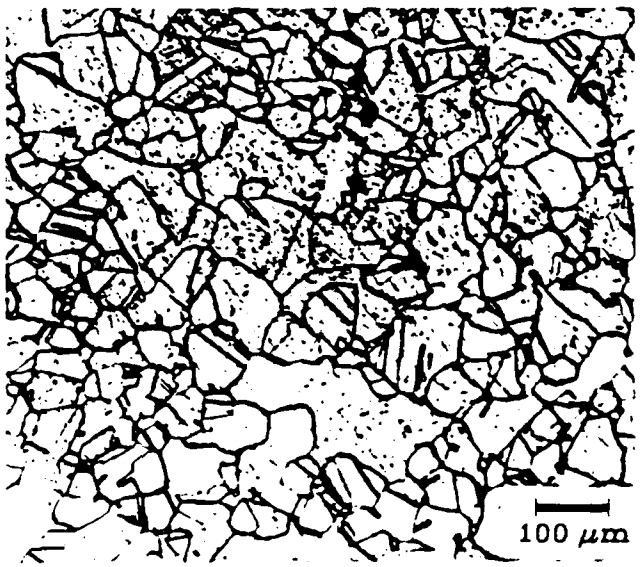

alloy 3S

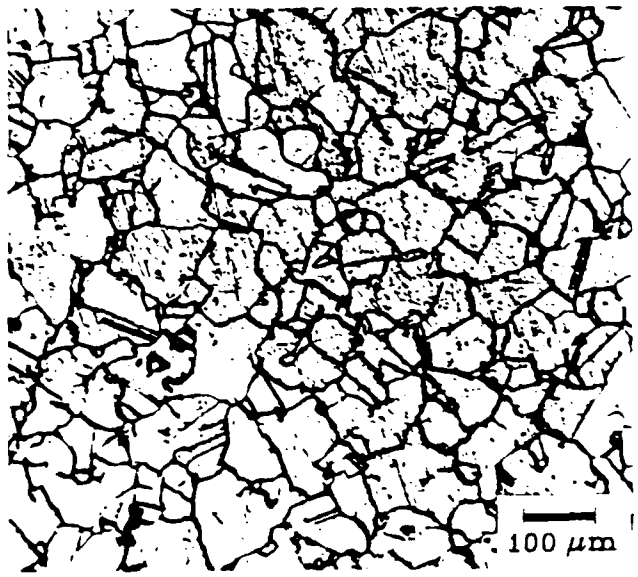

alloy 4S

Fig. 8 - Optical micrographs of initial small γ' alloy structures. Specimens etched for 30 seconds in 33% H_2O, 33% nitric acid, 33% methanol, and 1% HF acid.

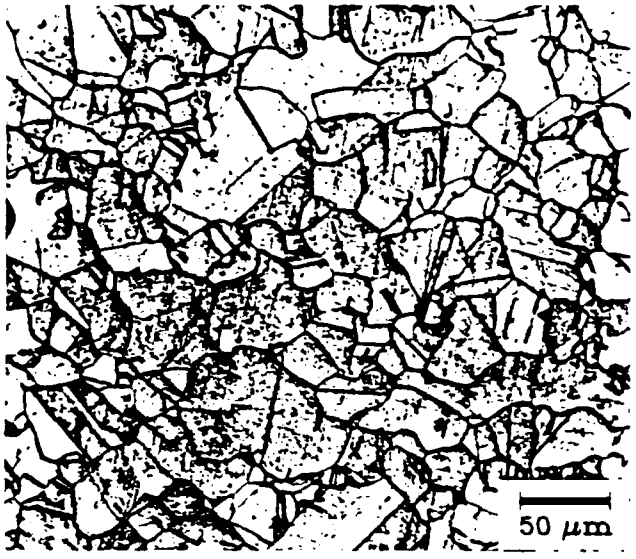

alloy 1L

alloy 2L

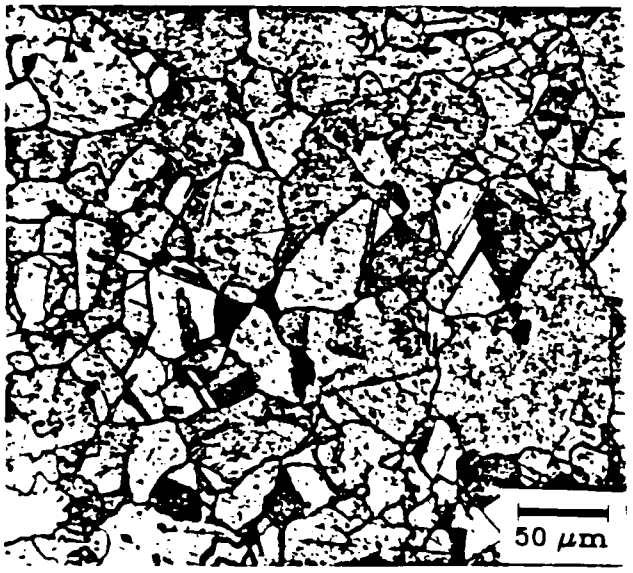

alloy 3L

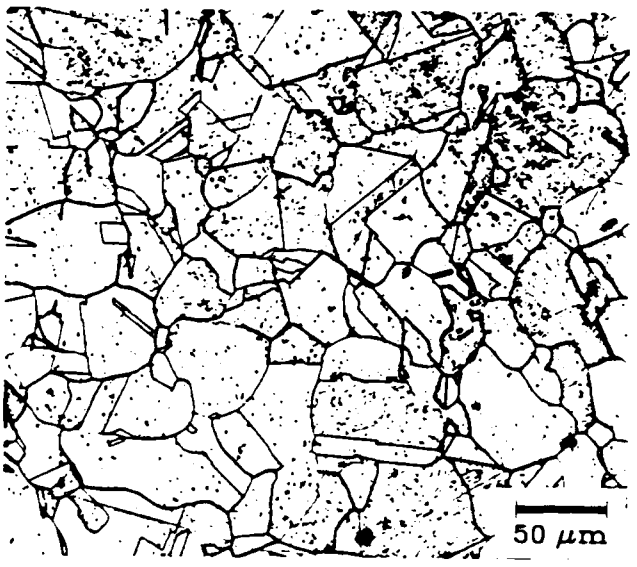

alloy 4L

Fig. 9 - Optical micrographs of initial large γ' structures. Specimens etched for 30 seconds in 33% H_2O, 33% nitric acid, 33% methanol, and 1% HF acid.

alloy 1S

alloy 2S

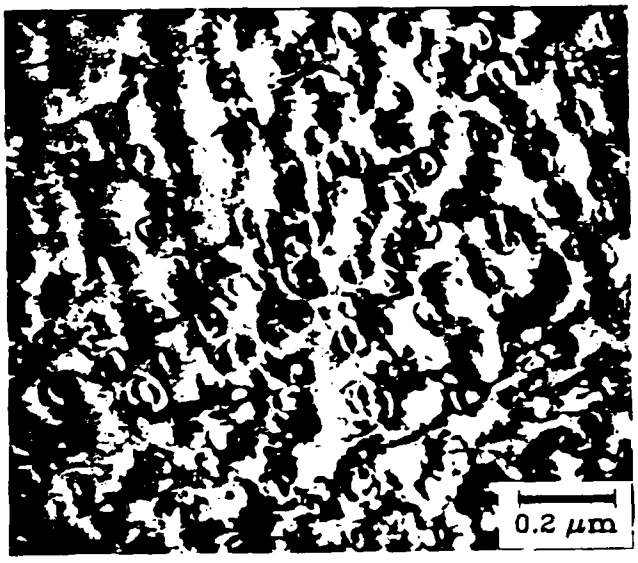

alloy 3S

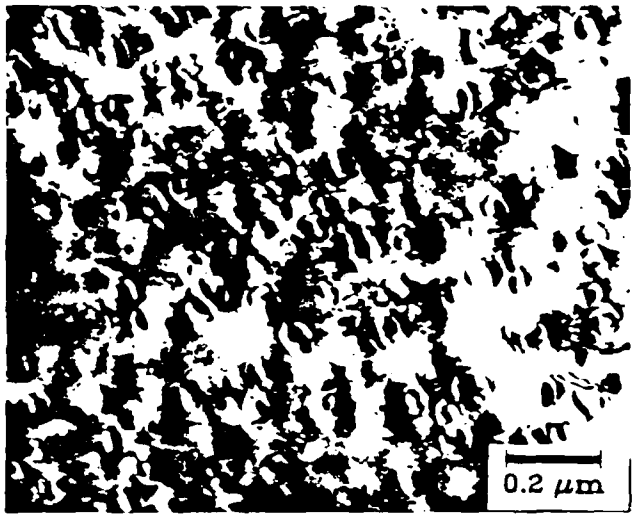

alloy 4S

Fig. 10 - TEM micrographs of small γ' alloy initial structures.

alloy 1L

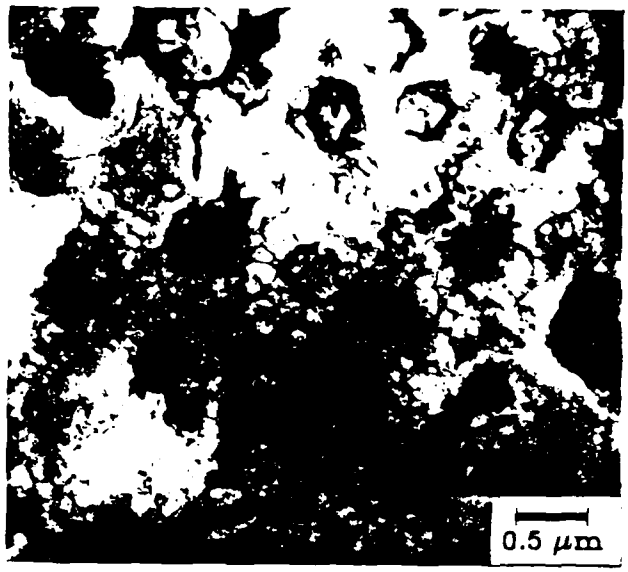

alloy 2L

alloy 3L

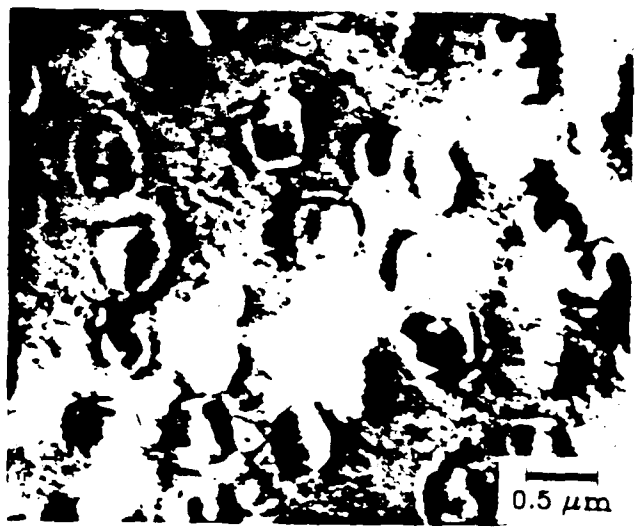

alloy 4L

Fig. 11 - TEM micrographs of large γ' alloy initial structures.

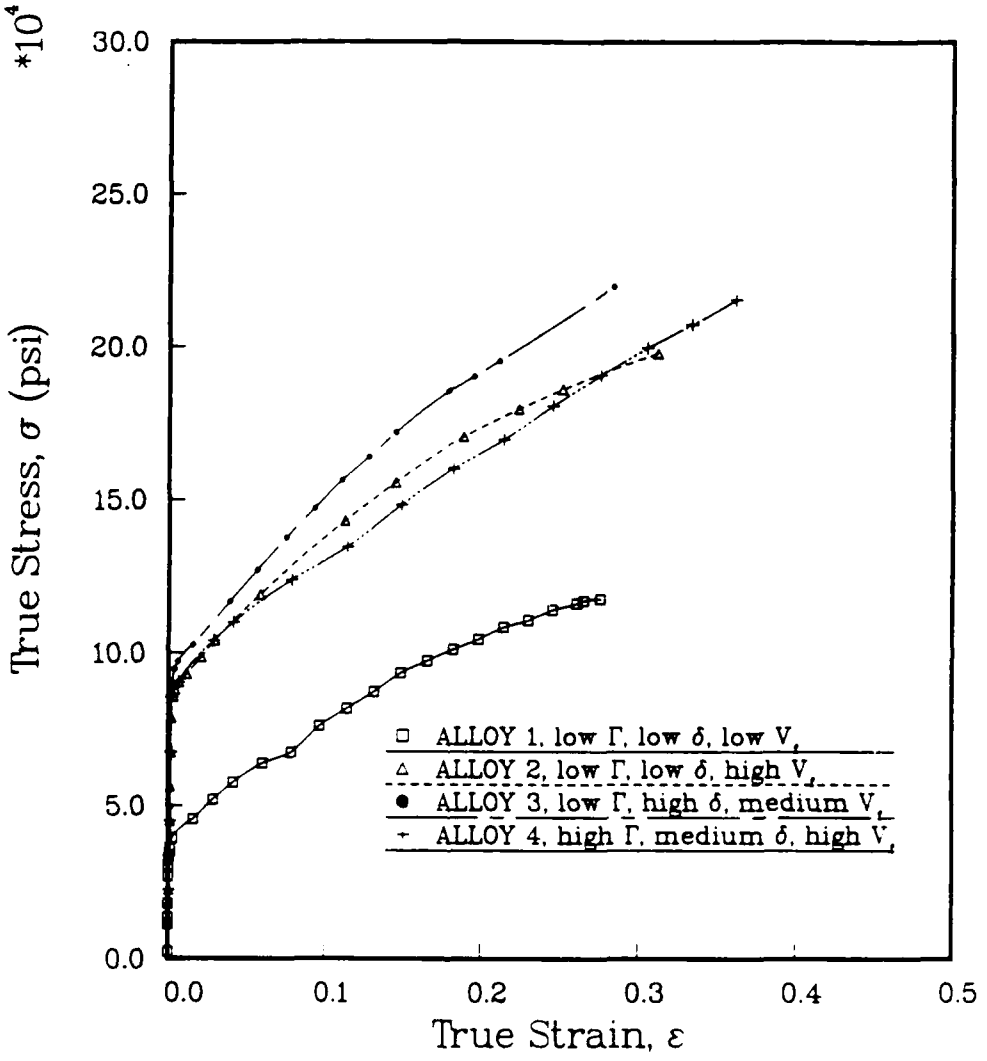

Fig. 12 - True stress-strain curves for small γ' alloys.

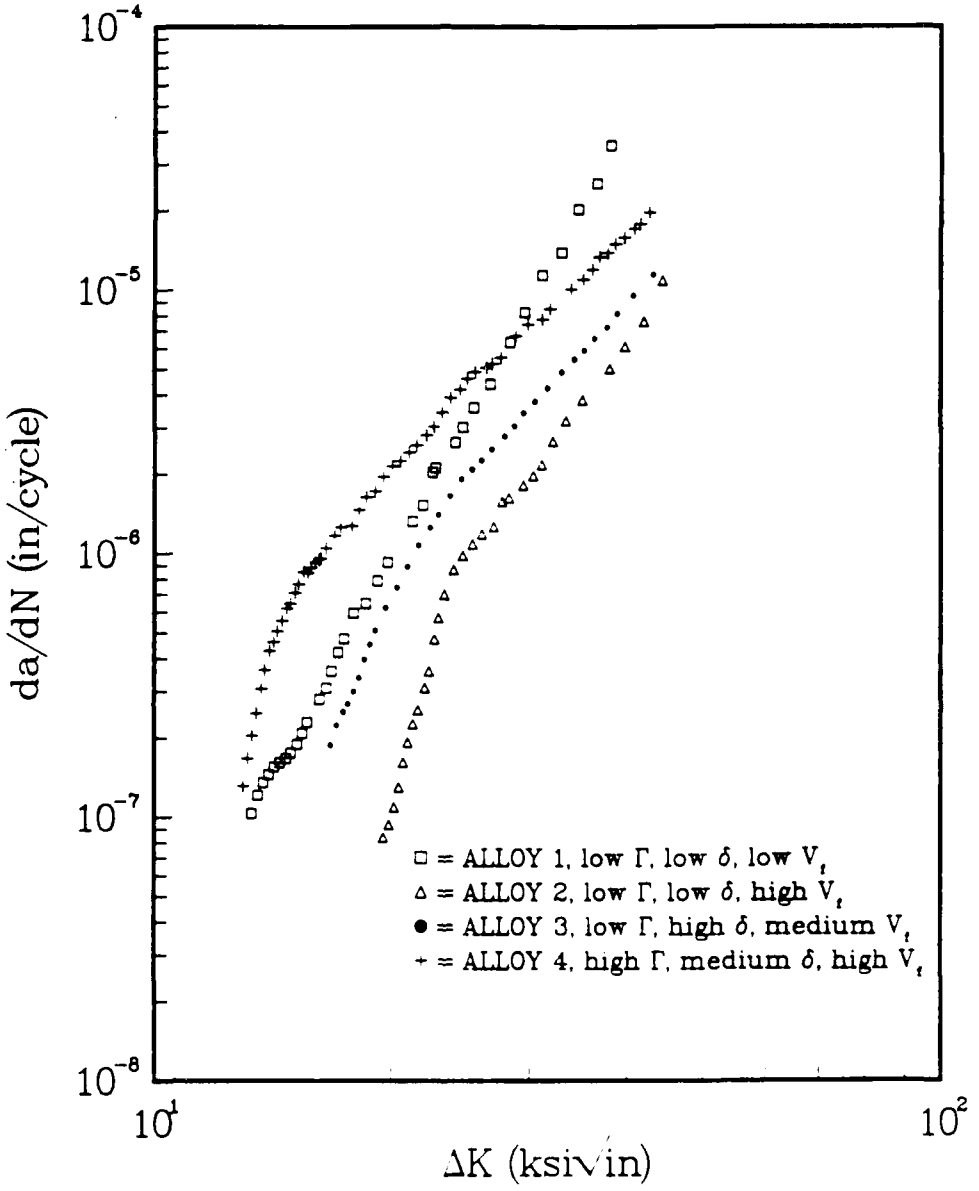

Fig. 13 - Fatigue crack growth curves small γ' alloys at R = 0.1.

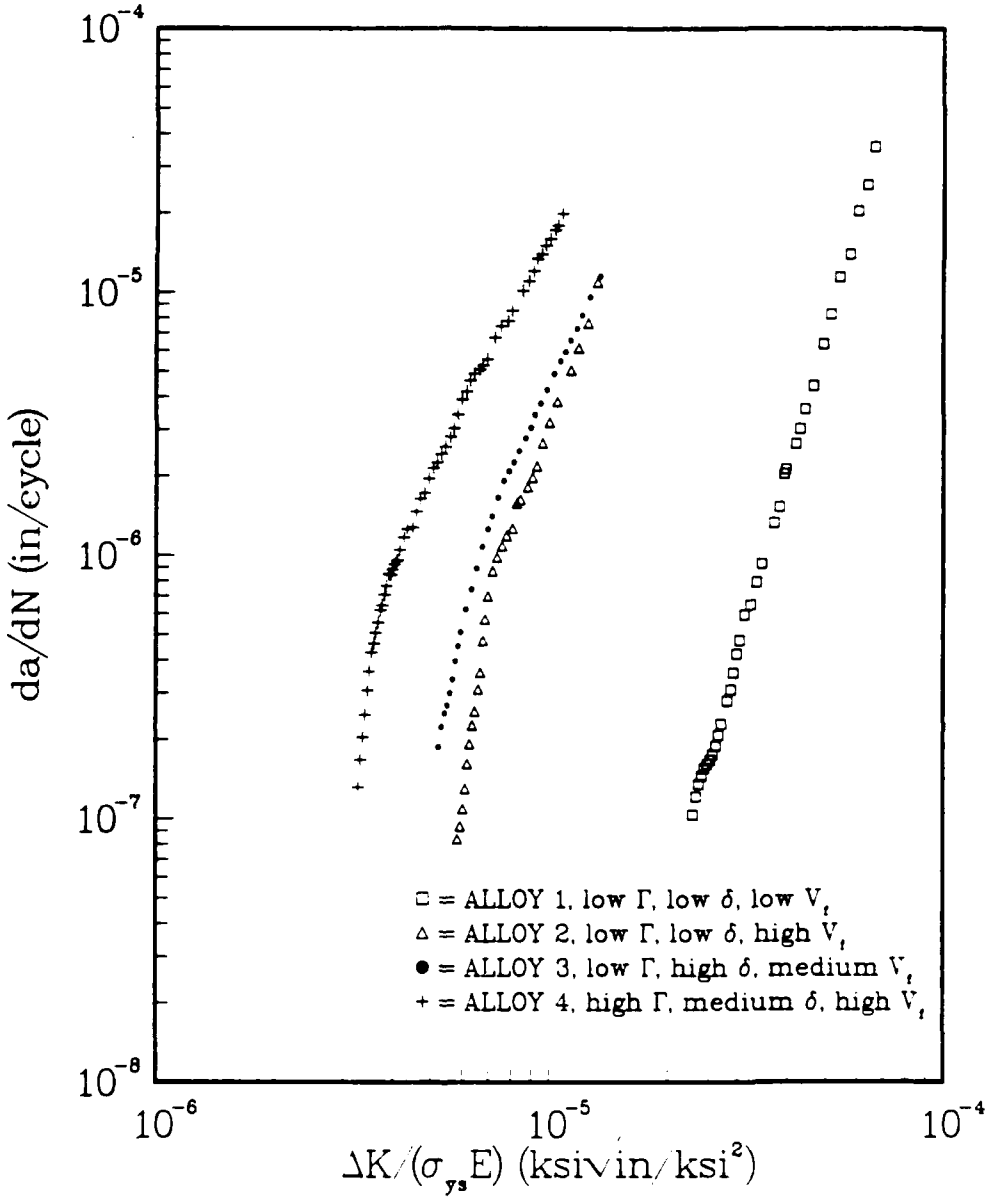

Fig. 14 - Fatigue crack growth rates at R = 0.1 for small γ' alloys normalized with respect to yield strength and elastic modulus.

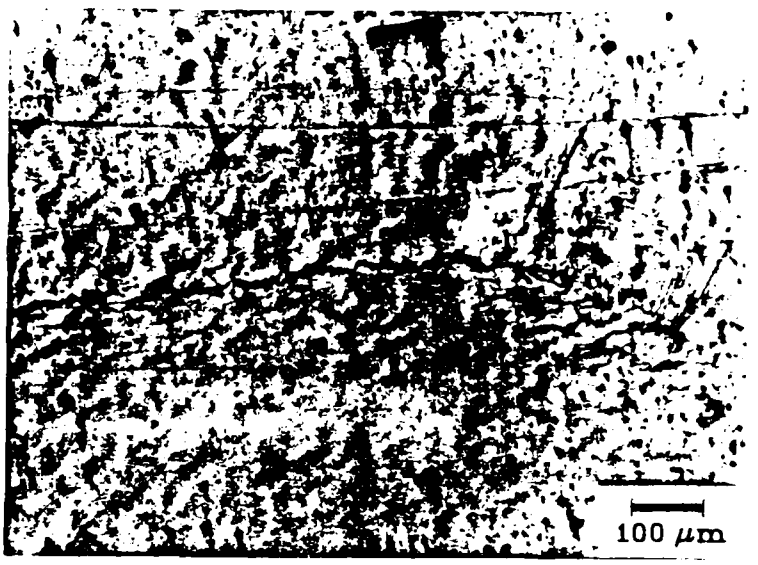

alloy 1S, R_f ~ 1

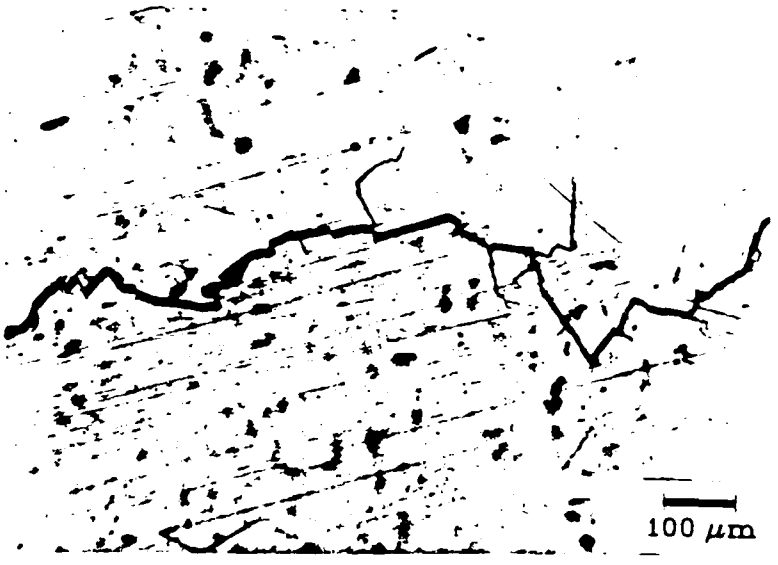

alloy 2S, R_f ~ 1.6

Fig. 15 - Optical micrograph of fracture surface profiles.

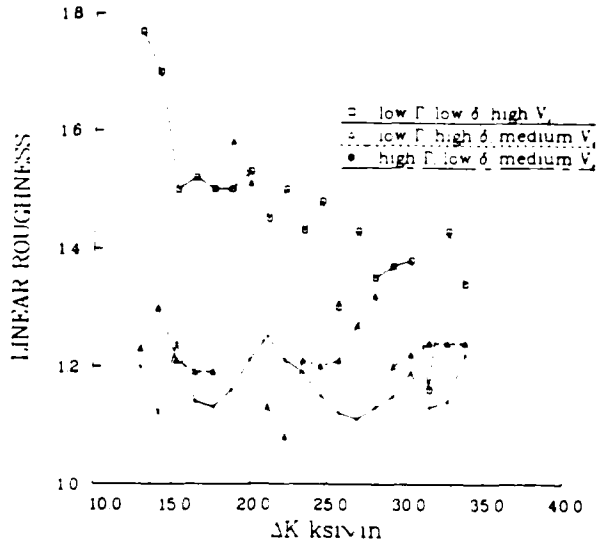

small γ' alloys

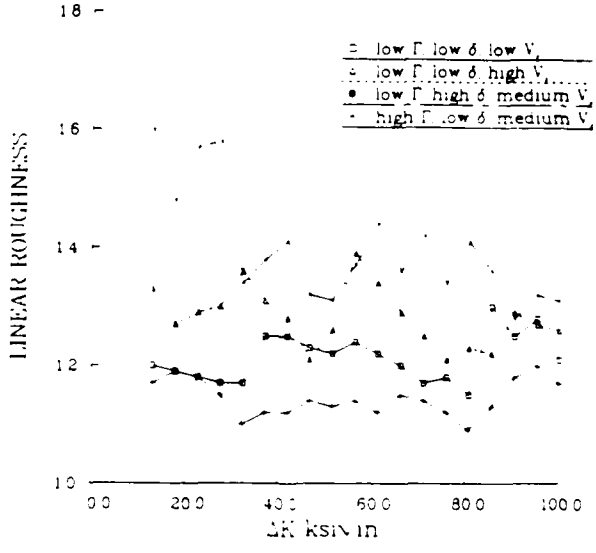

large γ' alloys

Fig 16. - Linear roughness parameter, R_f, of fracture surfaces.

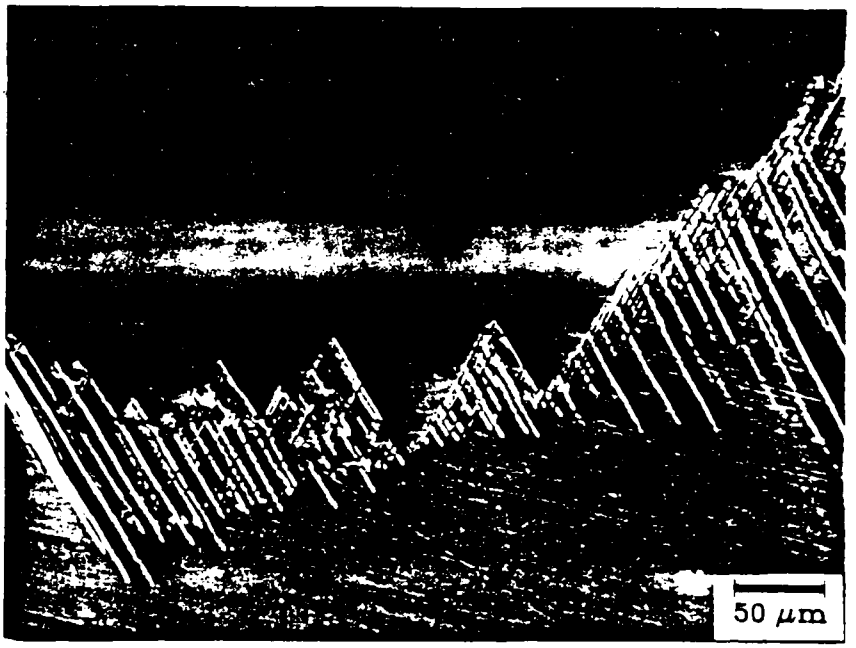

Fig. 17 - Fracture surface roughness arises due to cracking along slip bands in alloy 2S.

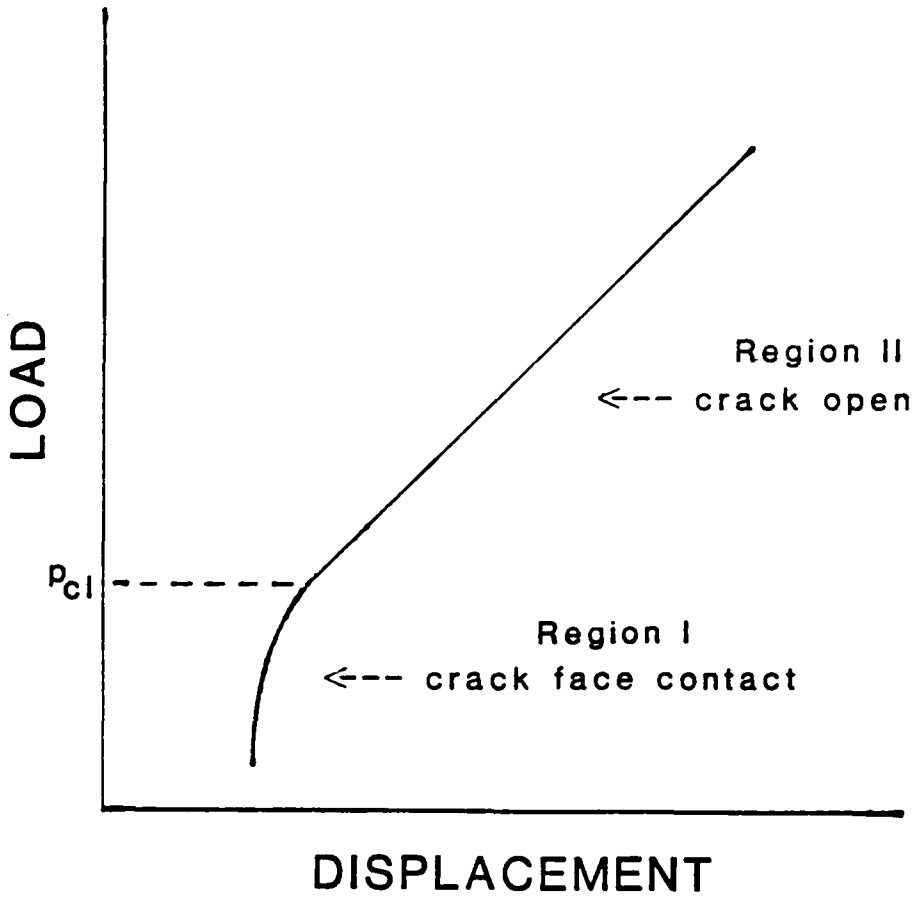

Fig. 18 - Schematic load-displacement curve used for measuring closure loads. P_{cl} is usually defined by the intersection of the extrapolated lines.

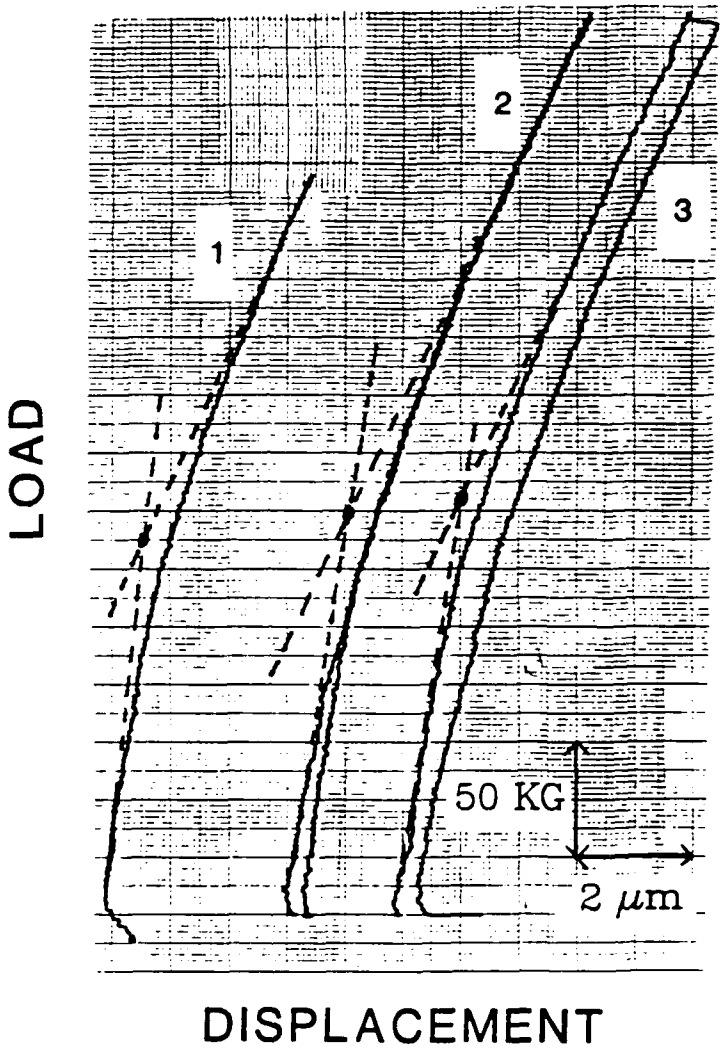

Fig. 19 - Load displacement curves for specimen with notch only. Measurements were taken with 1) back-face strain gage, 2) clip gage, 3) laser exstensometer.

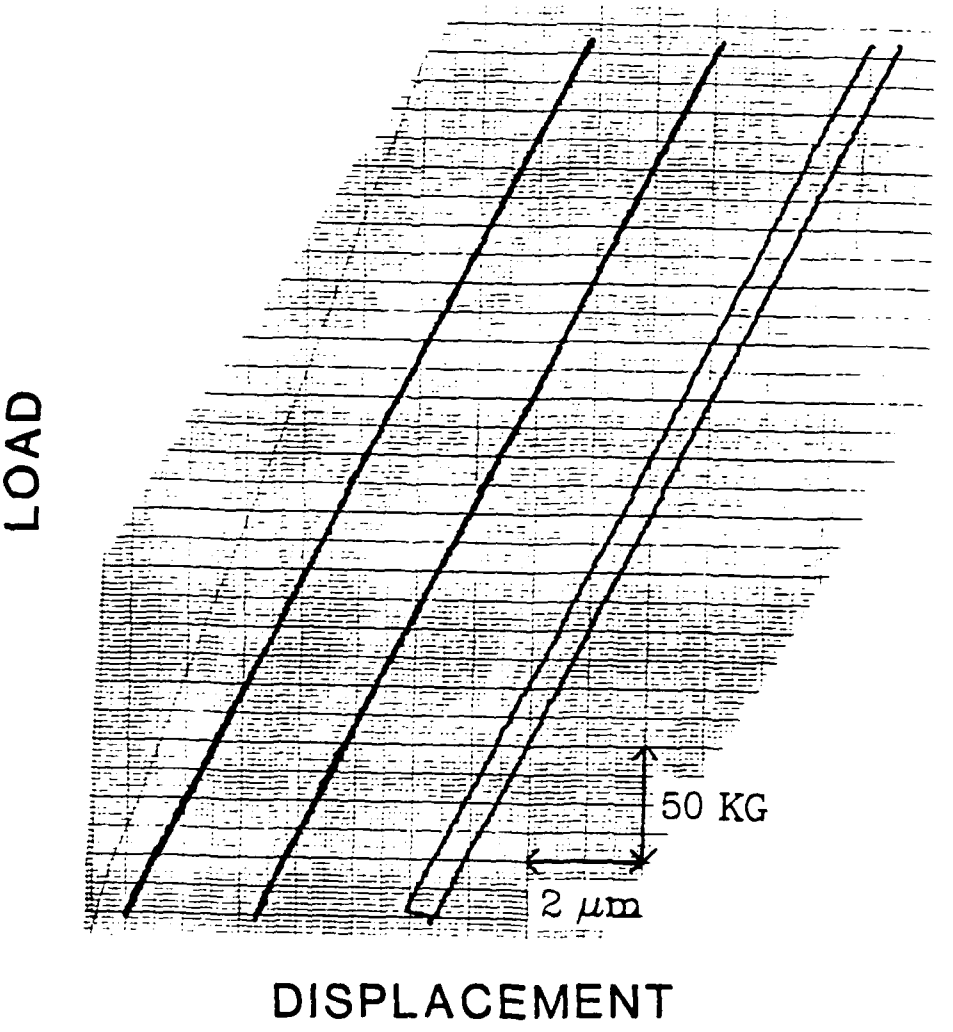

Fig. 20 - Load displacement output from laser extensometer after performing test modifications. Each trace represents several loading cycles which exactly retraced the previous one. Specimen was removed from the machine and reinserted four times to insure reproducibility.

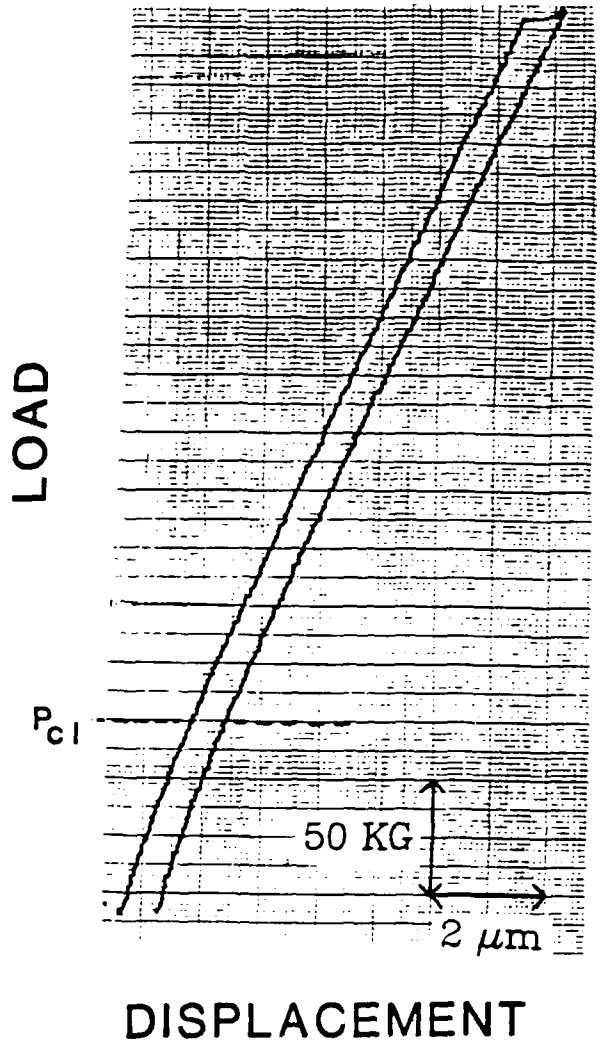

Fig. 21 - Load-displacement output from laser extensometer on a cracked specimen. Note linear region above the closure load.

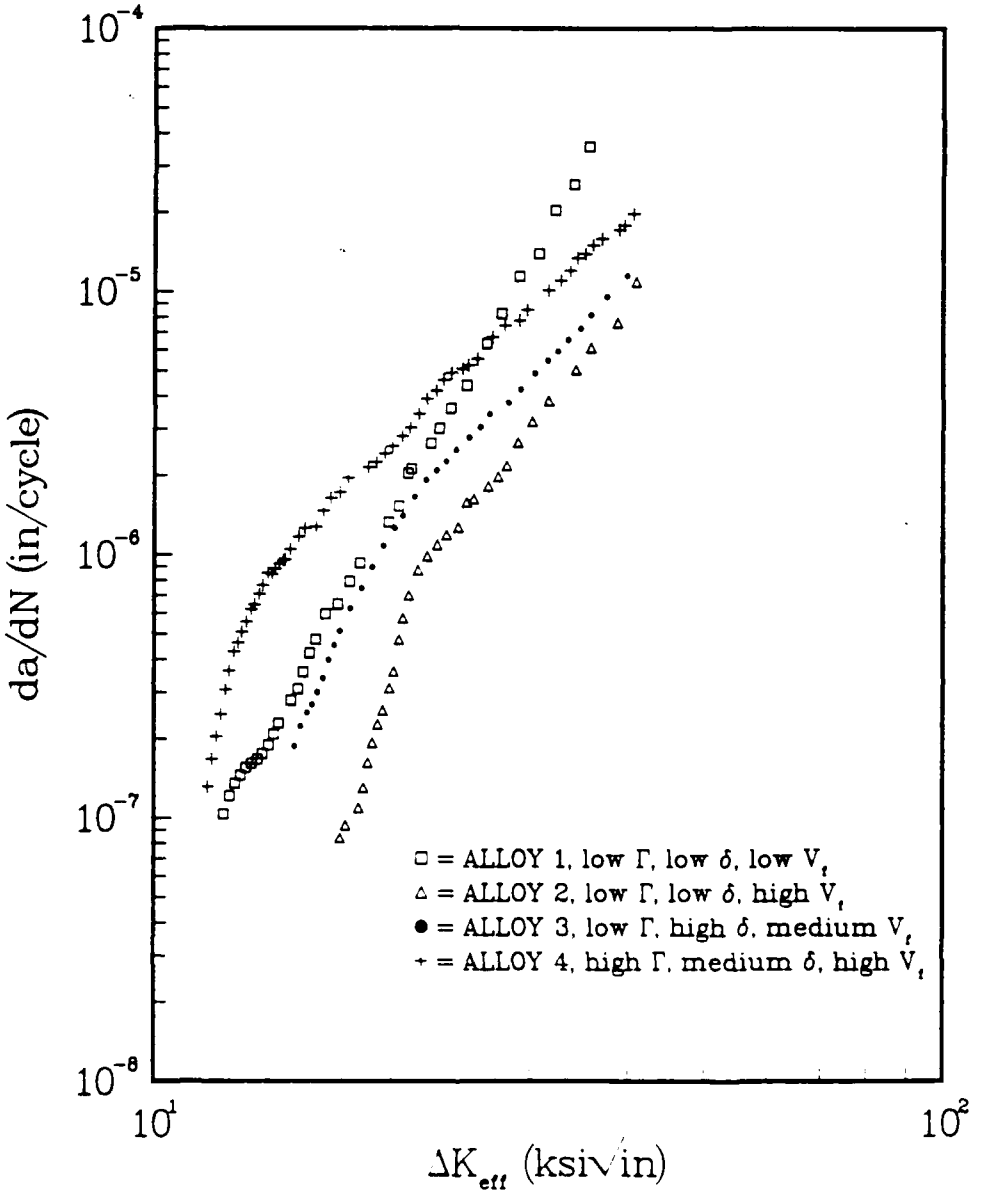

Fig. 22 - da/dN vs. ΔK_{eff} at R = 0.1 for small γ' alloys.

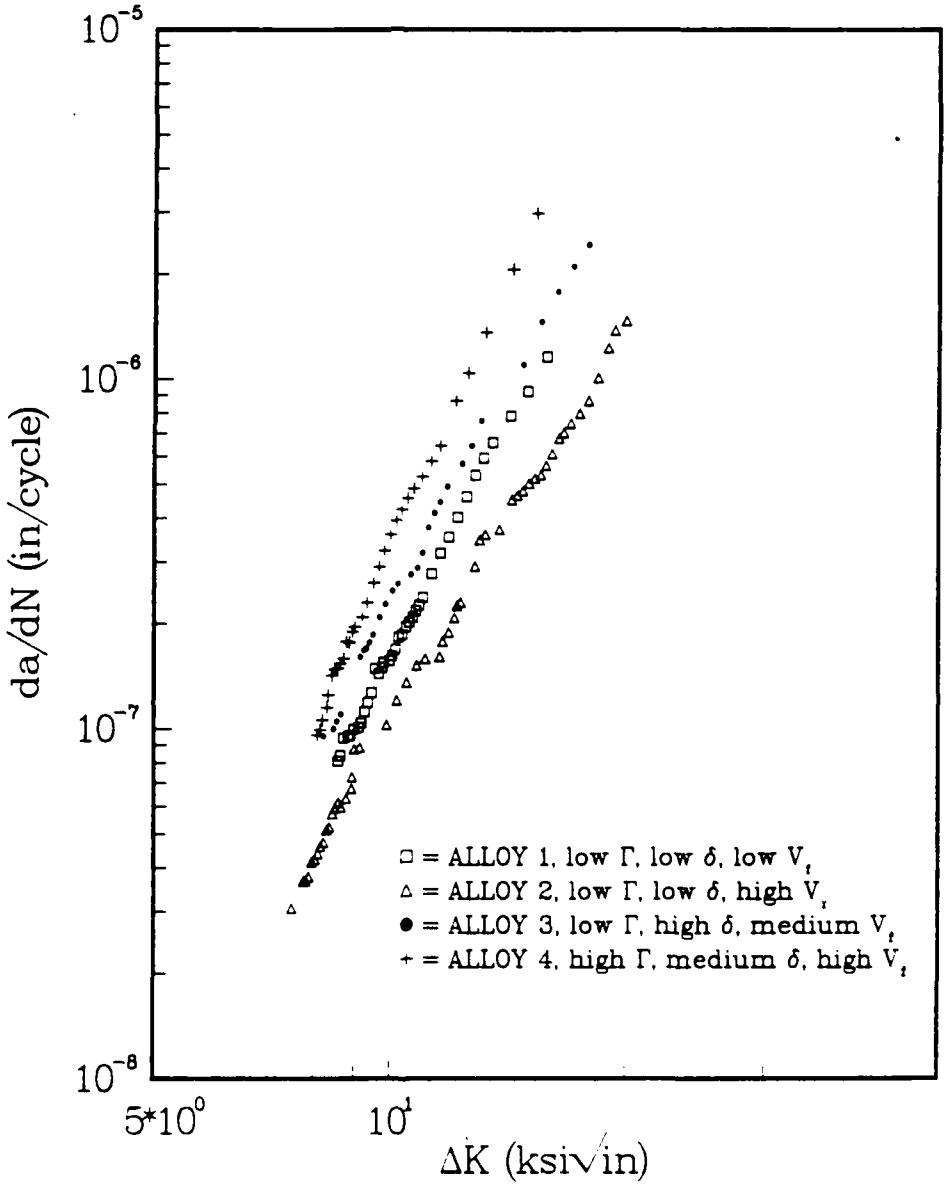

Fig. 23 - Fatigue crack growth response at R = 0.8 for small γ' alloys.

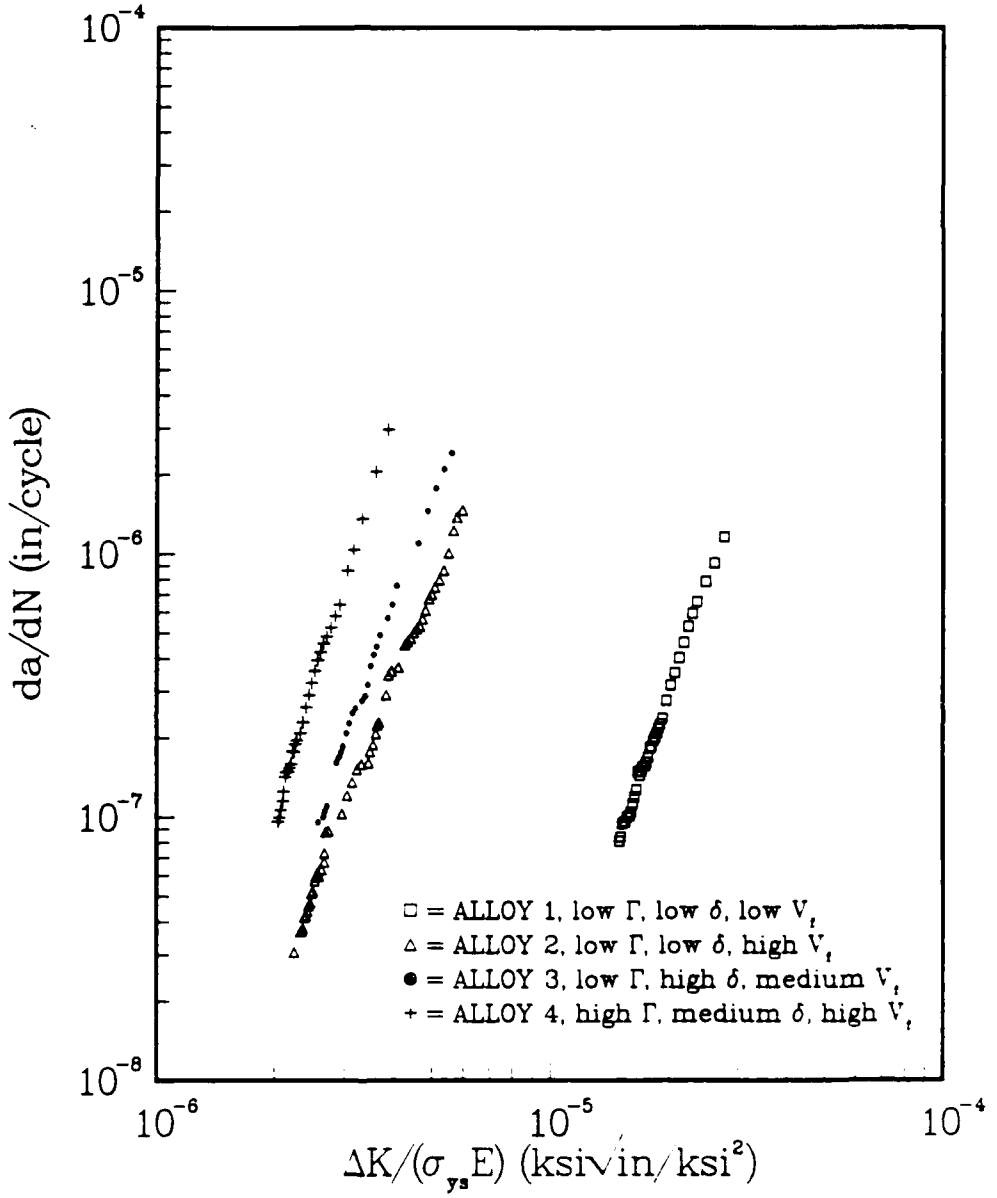

Fig. 24 - Fatigue crack growth response at R = 0.8 for small γ' alloys normalized with respect to yield stress and elastic modulus.

alloy 1S

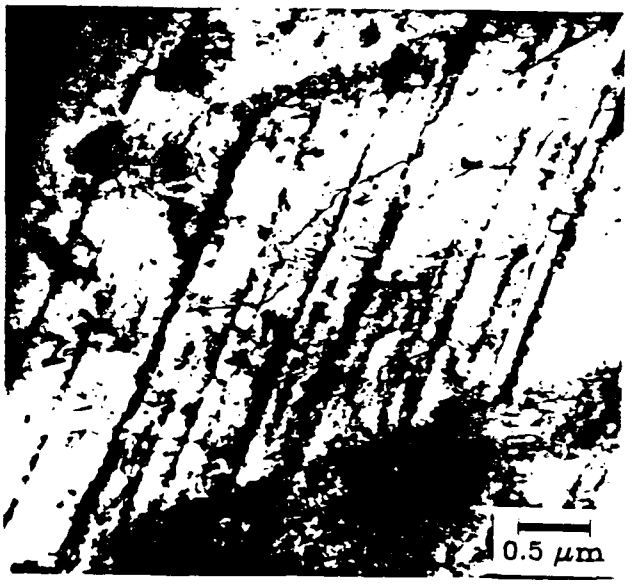

alloy 2S

alloy 3S

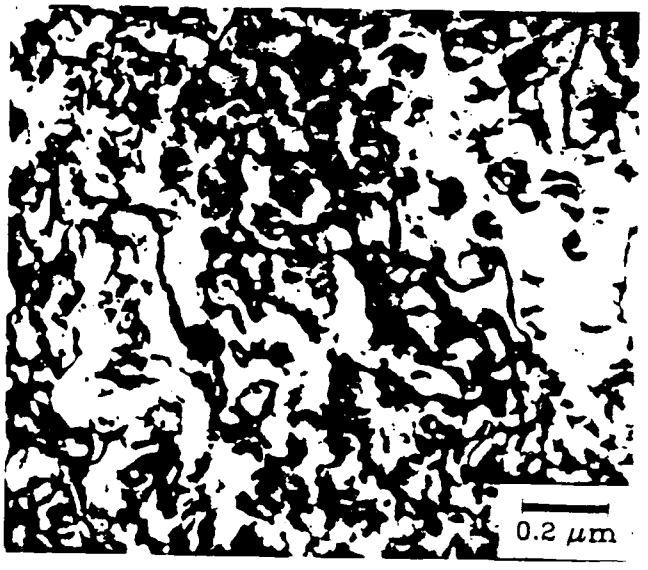

alloy 4S

Fig. 25 - TEM micrograph of LCF specimen cycled under total strain control (ε = 0.2%) to failure.

alloy 1L

alloy 2L

alloy 3L

alloy 4L

Fig. 26 - TEM micrograph of LCF specimen cycled under total strain control (ε = 0.2%) to failure.

Fig. 27 - TEM micrograph showing dislocation by-pass of large γ' particle.

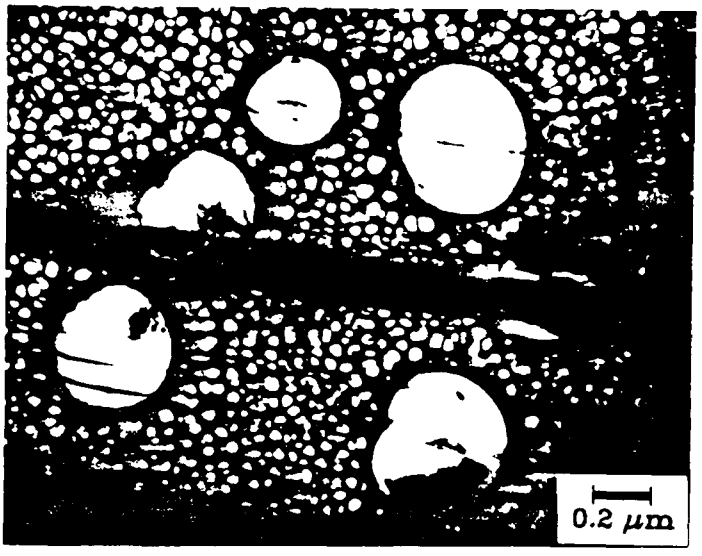

Fig. 28 - TEM dark field image of dislocation shearing large γ' particle.

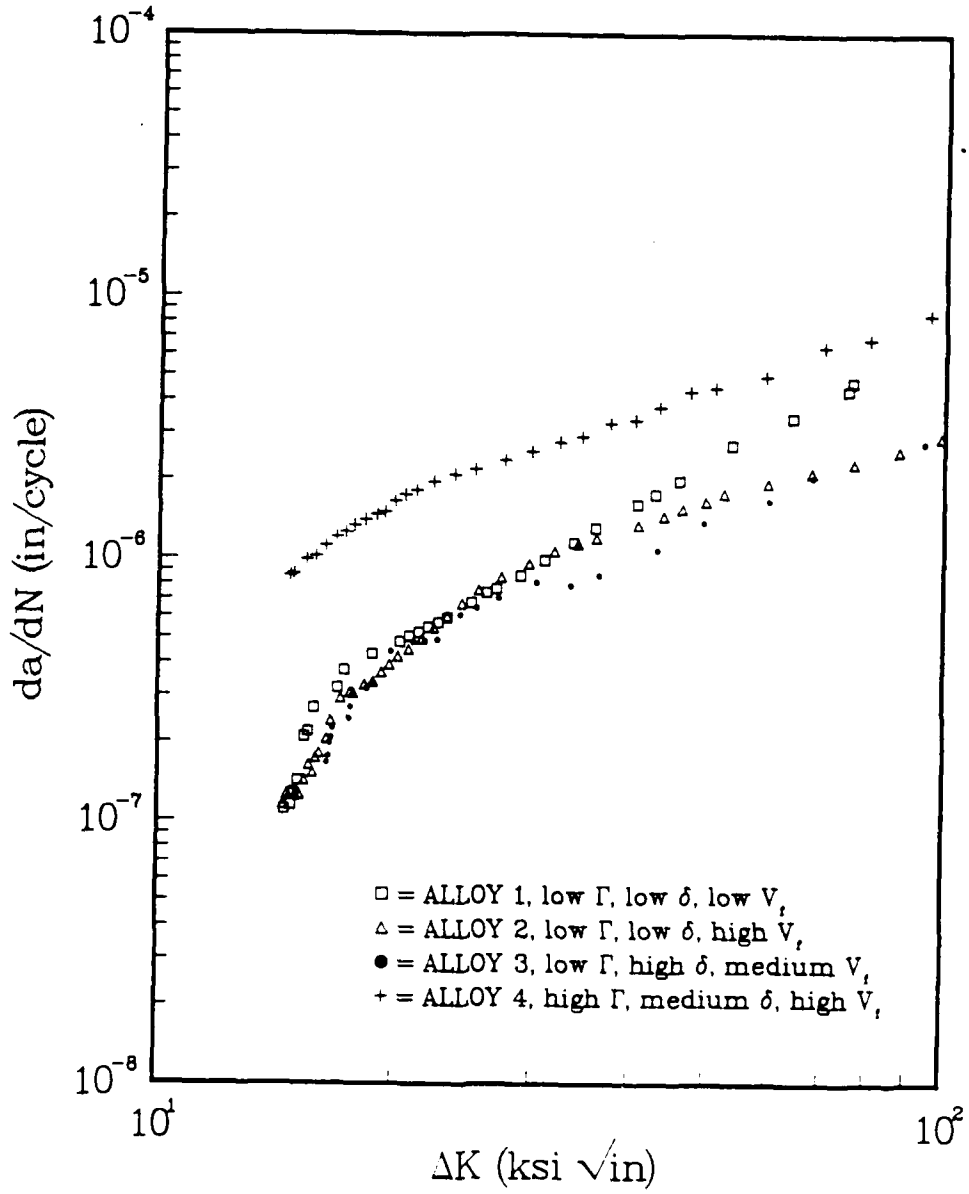

Fig. 29 - da/dN vs. ΔK at R = 0.1 for large γ' alloys.

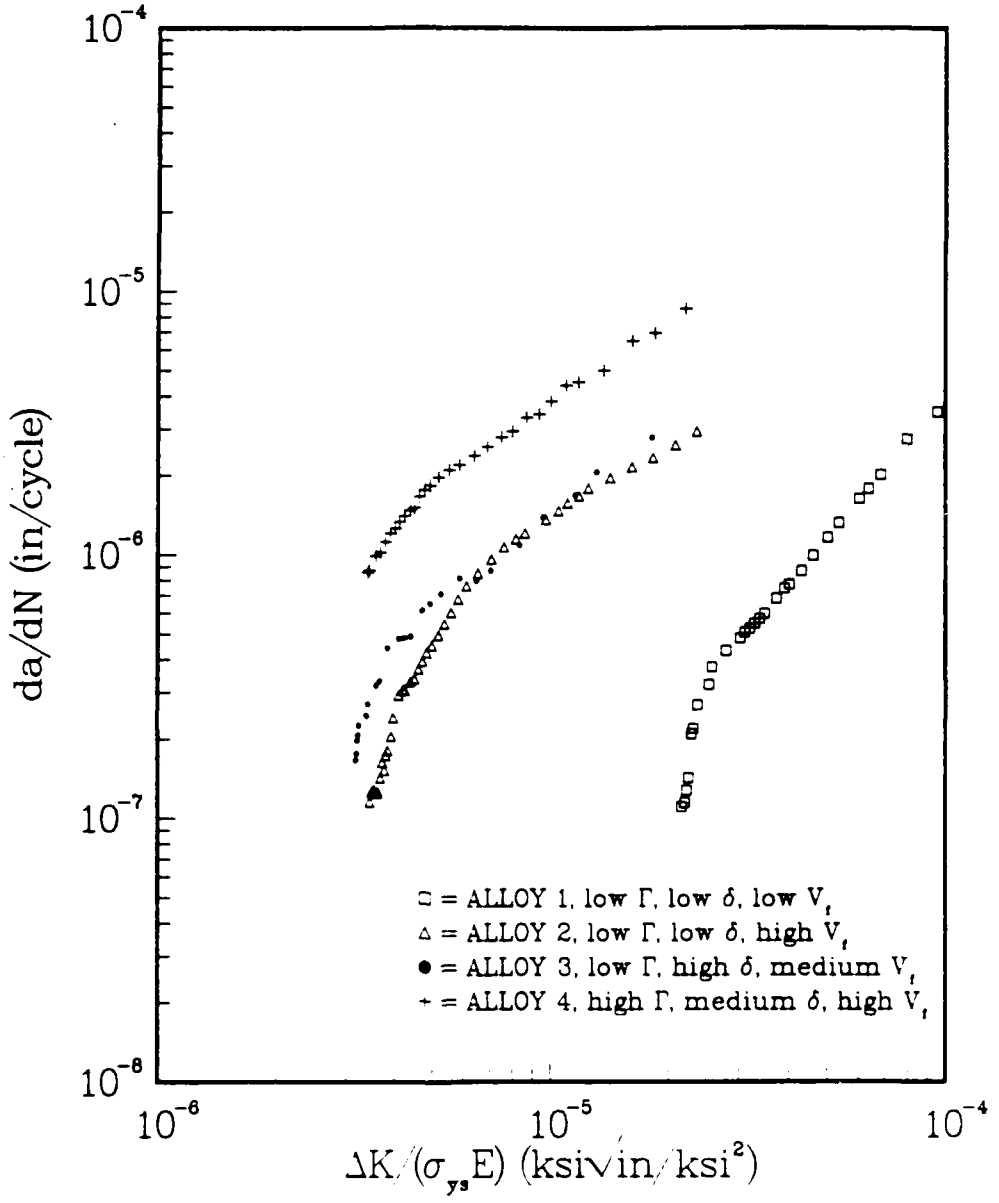

Fig. 30 - Fatigue crack growth rates at R = 0.1 for large γ' alloys normalized with respect to yield strength and elastic modulus.

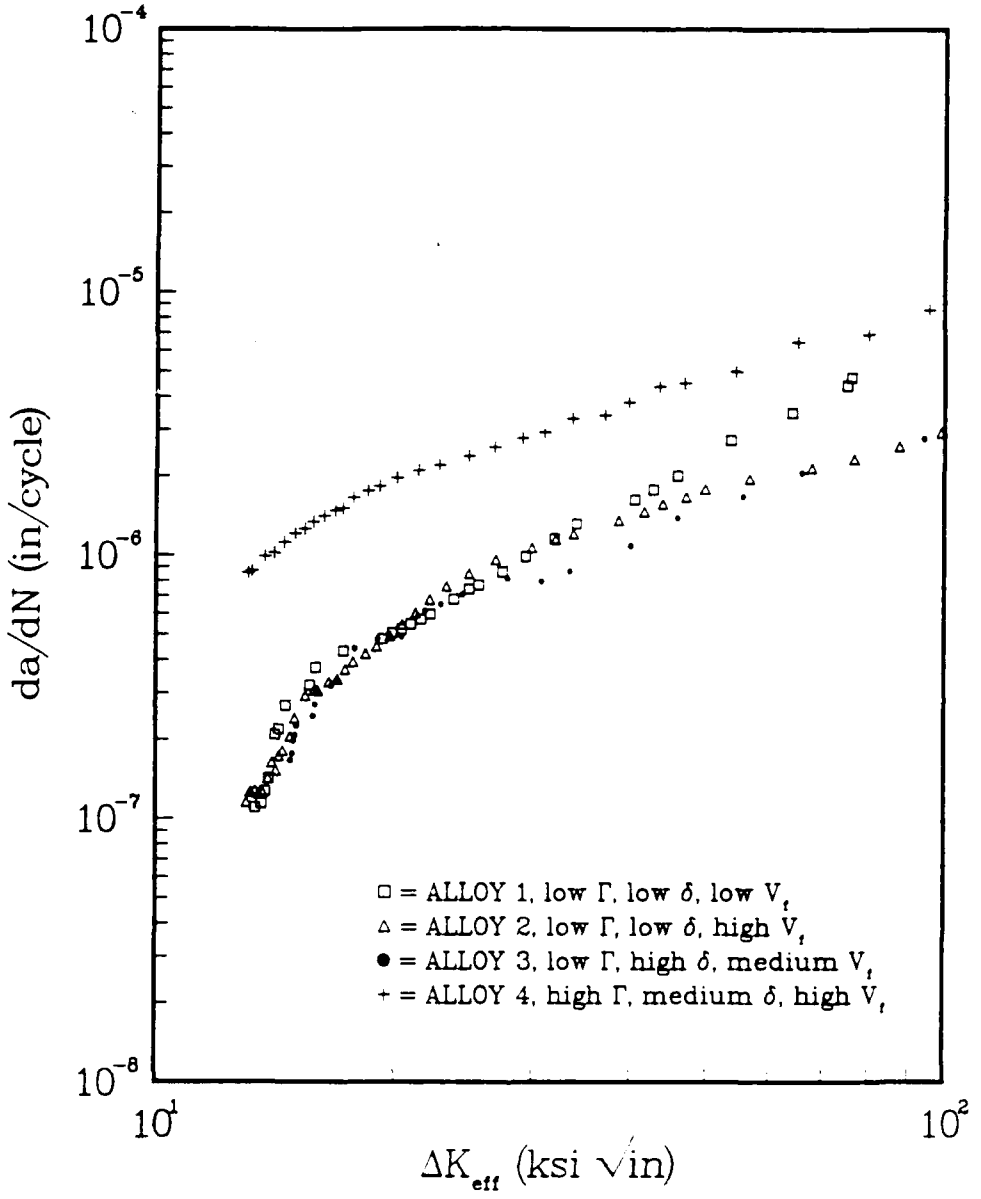

Fig. 31 - da/dN curve vs. ΔK_{eff} at R = 0.1 for large γ' alloys.

AD-A193 222 EFFECT OF MICROSTRUCTURE ON THE FATIGUE CRACK PROPAGATION BEHAVIOR OF NI-..(U) GEORGIA INST OF TECH ATLANTA SCHOOL OF MATERIALS ENGINEERING.. 2/2

UNCLASSIFIED S D ANTOLOVICH DEC 87 AFOSR-TR-88-0295 F/G 11/6.1 NL

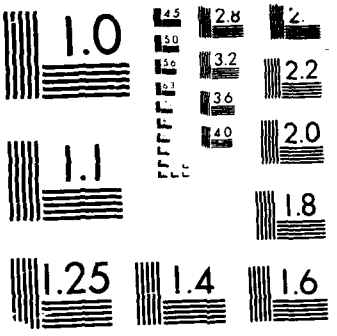

MICROCOPY RESOLUTION TEST CHART

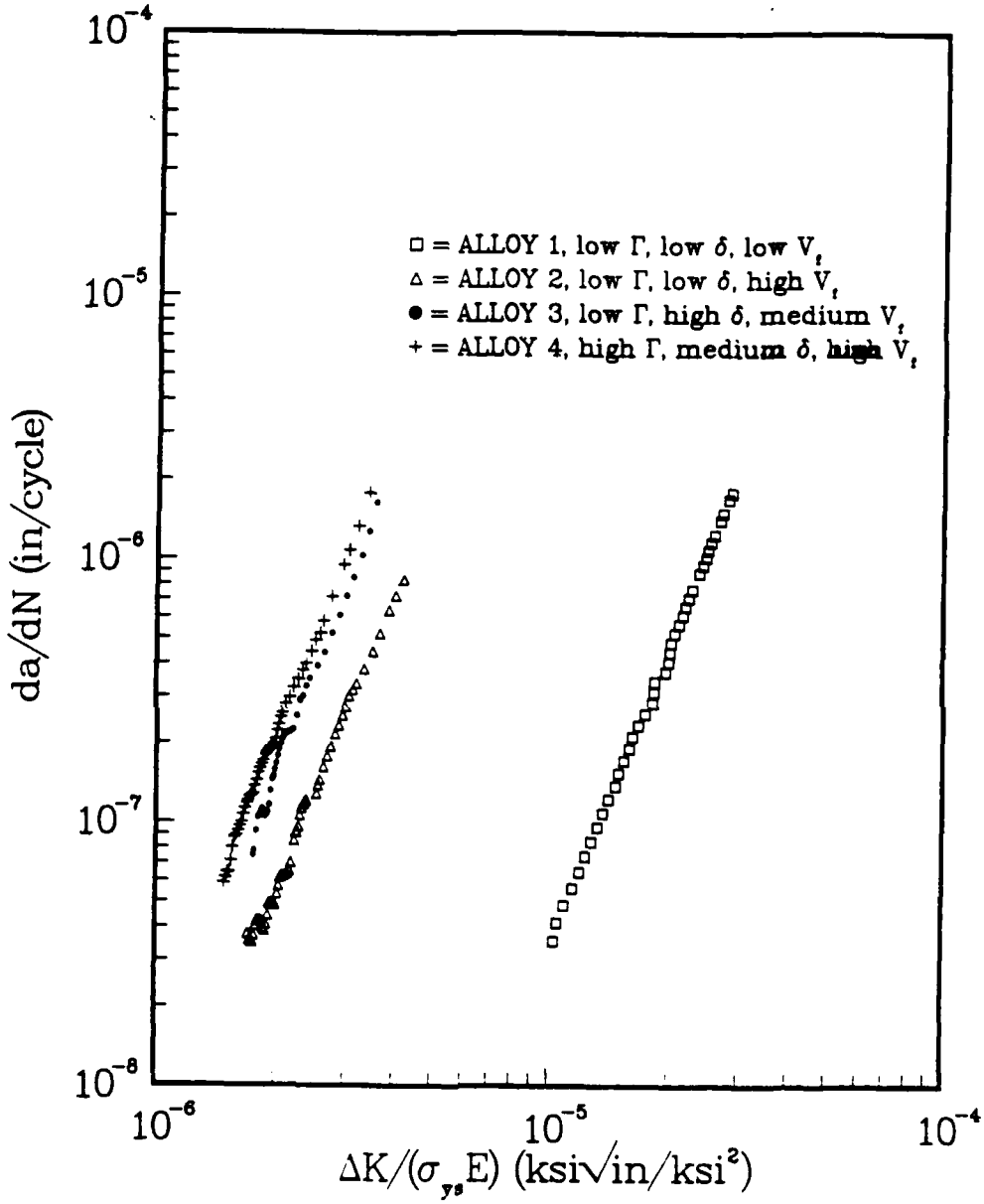

Fig. 32 - Fatigue crack growth rates at R = 0.8 for large γ' alloys normalized with respect to yield strength and elastic modulus.

TABLE I. Alloy compositions in weight percent.

							desired properties		
Alloy	Ni	Al	Ti	Mo	Cr	B	Γ	δ	V_f
1	Bal	2.35	<.01	<.01	13.83	.0037	low	low	low
2	Bal	4.92	<.01	<.01	14.18	.0042	low	low	high
3	Bal	2.96	2.58	<.01	9.39	.0037	low	high	low
4	Bal	1.24	3.71	9.91	13.21	.0060	high	low	high

alloy suffix designator

S : small γ' precipitates
L : large γ' precipitates

TABLE II. Measured microstructural properties

Alloy	grain size (μm)	γ' size (μm)	Γ (ergs/cm^2)	δ (%)	V_f (%)	σ_{ys} (ksi)	ε_f (%)
1S	5.2	0.08	75	.09	21	30.31	54.9
1L	5.5	0.50	75	.07	21	32.60	49.6
2S	5.1	0.09	75	.07	27	88.68	36.6
2L	5.2	0.62	75	.04	25	100.00	31.2
3S	3.6	0.07	75	.21	21	94.30	32.8
3L	4.2	0.54	75	.18	18	108.40	31.6
4S	2.3	0.07	141	.10	25	94.3	48.4
4L	3.4	0.68	131	.14	22	93.2	42.3

TABLE III. Closure loads at various ΔK levels at R = 0.8.

	closure load (P_{op}/P_{max})					
Alloy | ΔK :	20	30	40	50	60	70
1S	0.08	0.07	0.07			
1L	0.08	0.05	0.05	nil	nil	nil
2S	0.12	0.10	0.10			
2L	0.10	0.09	0.06	0.05	0.05	nil
3S	0.10	0.10	0.08			
3L	0.10	0.08	0.07	0.07	0.03	nil
4S	0.10	0.07	0.07			
4L	0.10	0.08	0.06	0.05	0.05	nil

END

DATE

FILMED

DTIC

JULY 88